Integrated Master in Chemical Engineering

Hydrogenation of styrene in Rotating Foam Reactors: Kinetic and mass transfer modelling.

Master Thesis

by

Bruno André Vilela dos Santos

Developed in the ambit of the course Dissertation

Realized in

Technische Universiteit Eindhoven

TU/e

Supervisor: **Prof. Dr. Ir. Xander Nijhuis**

Universidade do Porto
Faculdade de Engenharia
FEUP

Chemical Engineering Department

July of 2010

Index

Figure Index

Table Index

Abstract

In this work the hydrogenation of styrene catalyzed by palladium over alumina was studied in a rotating foam reactor. The activation energy of 54 *kJ* for this reaction was estimated by fitting the experimental data.

The catalyst consisted of aluminium foams, with different density cell, coated with alumina and impregnated with palladium. The foam structures were mounted on a stirrer shaft thus creating a catalytic stirrer with the purpose of overcoming the drawbacks of convectional slurry reactors, like catalyst separation and abrasion.

Then, the goal of the project is to study the liquid-solid mass transfer in this type of reactor and the influence of foam cell density and stirring speed on that.

Foam catalysts were successfully prepared by anodization, washcoating and palladium impregnation. An average thickness of 17, 24 and 35 μm was found for 10, 20 and 40 ppi foams, respectively. A homogenous coating was confirmed by SEM analysis. A good palladium distribution was confirmed by TEM analysis, with a narrow particle size distribution. Furthermore, for the 3 different ppi foams the average diameter of Palladium particles calculated was 2.2 *nm*.

In order to estimate liquid-solid mass transfer coefficient in the hydrogenation of styrene, it was necessary to confirm the absence of gas-liquid and internal mass transfer resistances. Therefore, experiments were performed at 60 ºC, 15 bars of hydrogen pressure and with one and two active blades. At these operating conditions were firstly proved that external mass transfer controls the overall reaction rate. With one and two active blades it was observed that the reaction activity was proportional to the liquid – solid surface area. Then, the reaction rate was controlled by liquid – solid mass transfer.

Therefore, an external mass transfer study was done in order to compare the design of reactors, the slurry and the rotating foam reactor. Values for the liquid – solid mass transfer coefficient found in common industrial slurry reactor are around 10^{-4} ms^{-1}. In the reactor used the two foams blades promote the agitation and the reaction due to the Palladium impregnated on the foam.

The liquid – solid mass transfer for the rotating foam reactor was estimated around 0.5 x 10^{-4} and 2.5 x $10^{-4} m.s^{-1}$, which is similar to the slurry reactor. A trend of decreasing the liquid – solid mass transfer coefficient, at the same stirrer speed, was observed with increasing of the foam cell density. This is related with the resistance to the convective flow. The small pores in high density cell foams promote highs pressures drop than larges porous. Consequently, the internal velocity for the same stirrer speed is lower.

Keywords: Heterogeneous catalyst, rotating foam reactor, liquid – solid mass transfer, multiphase reactor, styrene hydrogenation.

Acknowledgments

Over these 5 months developing this project I had one of the best experience of my life, personal and professional.

Starting with the professional environment, I am very glad for all the staff that worked with me, from SCR - Chemische Reactortechnologie. Starting from the all the technical team that has supported me in my experiments, and Dr. Ir. Xander Nijhuis, who with experience in the field, had helped me to make the best choice to orient my project. I want thank also to Roman for all the support and funny moments that we pass.

And the special person that was more than a supervisor, Maria Leon, who supports me and shared with me a lot of good moments. All this good environment that I found here, made me fell in home, and that was very important to my integration and my stability to do my best.

For all my friends and family from Portugal, who are always with me, I have to thank all the support and confidence that they have in me. For this reason they are my motivation in the hard days.

For all my new friends that I made here, in Erasmus, that give me very good moments help me to grow a little more with all this experience.

I want to thank especially to Bernardo, Chico and Pedro. They are my men companies like "DARTAGNAN E OS TRÊS MOSQUETEIROS". Also for my housemates Rocco, the best Italian guy better known as Dragon, and Amit, who pass a lot of time sleeping bad due to the party that I made at home.

For my 3 favorites girls, Elly, Ale, Oly, for whom a have I special affection and an infinite friendships and I will remember them forever.

Of course I can't forget the French Team: Guillaume, Thibault, Eric, Hicham, that always had time to drink a beer with me. Also Adelie and Paulline.

And also my two favorite Spanish's girls: Lourdes and Marta and Antonio (he know why I call him girl), my good friend from Turkey Emrah and Belu from Argentina, who never like to speak with me in Spanish.

And of course the Portuguese guy, Carlos that thinks that he is a football coach and will cry for me as soon as I leave.

Thanks to everyone and sorry if I forgot someone.

Nomenclature

Roman Symbols

$(-r_i)$	Reaction Rate of components *i*,	$mol.m^{-3}_{Reactor}.s^{-1}$
k	Reaction Rate Constant,	$m^3_{LS}.m^{-3}_{R}.g_{cat}^{-1}.s^{-1}$
k_0	Pre-exponential Factor,	$g_{cat}^{-1}.s^{-1}$
Ea	Activation Energy,	$J.mol^{-1}$
R	Ideal gases constant,	$J.K^{-1}.mol^{-1}$
T	Temperature,	K
K_{Sty}	Adsortion constant of styrene on palladium,	$m^3_{Liquid.Cat}.mol^{-1}$
C_i^s	Concentration of component *i*, on solid surface,	$mol.m^{-3}_{Liquid.Cat.}$
V_R	Reactor Volume,	$m^3_{Reactor}$
t	Time,	seg
k_{ls}^i	Liquid-solid mass transfer coefficient for component *i*,	$m_{Liq\text{-}Sol.}.s^{-1}$
k_{gl}^i	Gas-Liquid mass transfer coefficient for component *i*,	$m_{Liq\text{-}Sol.}.s^{-1}$
a_{ls}	Liquid-solid volumetric surface,	$m^2_{Liq\text{-}Sol}.m^{-3}_{Liquid}$
C_H^{sat}	Saturation concentration for the hydrogen solubility	$mol.m^{-3}_{Liquid}$
C_i^b	Concentration of component *i* on liquid bulk,	$mol.m^{-3}_{Liquid}$
L	Length average of catalyst porous,	m
D_i	Diffusion of component *i*, in Toluene,	$m^2.s^{-1}$
D_{eff}^i	Effectiveness Diffusion of component *i*, on the catalyst,	$m^2.s^{-1}$
p_H	Hydrogen Pressure,	MPa
H	Henry's Constant,	$MPa.\ m^3_{Liquid}.mol^{-1}$
W_{cat}	Catalyst mass,	g_{cat}
V_m	Solute molar volume at normal boiling point,	$m^3.kmol^{-1}$
M	Molar mass,	$kg.kmol^{-1}$

Greek symbols

ε_G	Gas Fraction,	$m^3_{Gas.}.m^{-3}_{Reactor}$
ε_L	Liquid Fraction,	$m^3_{Liquid.}.m^{-3}_{Reactor}$
ε_S	Solid Fraction,	$m^3_{Solid.}.m^{-3}_{Reactor}$

ε_{cat}	Foam porosity,	$m^3_{Liquid.Cat}.m^{-3}_{Solid}$
η_i	Efficiency factory of catalyst for component *i*	
ϕ_i	Thiele's Module for the component *i*	
μ	Viscosity	*Pa.s*
θ	Parameter associated to the solvent, equation (3.3)	
λ	Latent heat,	$kJ.kmol^{-1}$

Subscripts

i	Hydrogen (*H*) or Styrene (*Sty*) Component
LS	Liquid – solid interface
L	Liquid
G	Gas
S	Solid
Cat	Catalyst
Sty	Styrene
H	Hydrogen
Eff	*Effectiveness*
m	*molar*

Abbreviations

SEM	Scanning Electron Microscopy
TEM	Transmission Electron Microscopy
ppi	Porous per inch
PYNGAS	Pyrolysis gasoline

1. Introduction

1.1. Slurry reactors and structured catalyst reactors

In the chemical industry it is common to find a lot of heterogeneously catalyzed gas – liquid reactions. A large wide of reactors types are available to carry out these reactions. One of the biggest problems of operating industrial reactors is on the mass transfer resistance. Usually this resistance is present and affects the good performance expected of the reactor.

In order to increase the mass transfer, a lot of multiphase reactors configurations are designed, as packed bed, trickle bed, bubble column, slurry reactors, and monolithic reactors, among others. Some strategies presented by Krishna [1] are useful to choose the better hydrodynamics flow regime.

In batch reactions, the most common reactor used is the slurry reactor, because these reactors are very versatile, they have a high specific area which promotes high activity and lower mass transfer resistance. However, there are some disadvantages related to this configuration. First, they have high operating costs associated to the filtration process for separating the catalyst. In addition, the catalyst particles can agglomerate and create hot spots if the reaction is highly exothermic. Moreover, the abrasion of the particles when they impact to the wall or with the stirrer can occur quite often.

With the aim of avoiding these problems, other reactor configurations are developed that use structured catalyst supports. One example is the monolithic reactor which has received a lot of attention in industrial process. Although these reactors can avoid these problems, they have some disadvantages. For instance, they have less area per volume than the slurry catalyst, consequently, lower activity.

In literature [2,3], it can be found correlations to predict the mass transfer coefficients for those systems.

Nijhuis et al. [4] compared the performance of a monolithic and a trickle bed reactors. They reported that the monolithic reactor could reach higher productivity and selectivity than the trickle bed reactor. In addition, this type of structure shows low pressure drop, and therefore they could be a good replacement for slurry and packed bed reactors.

Other study [5] compared the power consumption for stirring between the monolithic catalyst and the Rushton stirrer, normally used in slurry reactors. It was concluded that monolithic catalyst spends more power input for the same stirrer speed. However, a more deep study must be done in order to conclude which process is more economical attractive.

Structured catalysts also have promising applications for selective reactions as the hydrogenation of functionalized alkynes. The hydrogenation of 3-methyl-1-pentyl-3ol has been used as a model reaction for hydrogenation of functionalized alkynes. The objective is to maximize the yield of alkenes production.

Nijhuis et al. [6] carried out this reaction over palladium on silica support, the solubility of the hydrogen was estimated by the IUPAC data. They concluded that the internal mass transfer resistance were present which influenced the selectivity.

Structured catalyst, as monolithic catalyst shows highs selectivity, for this reaction [5]. Nijhuis et al. [7] also compared the selectivity of a monolithic stirrer including the effect of quinoline concentration and the usage of a bimetallic palladium-copper catalyst. They demonstrated that the monolithic catalyst reaches high selectivity as a consequence of the shorter diffusion distances inside the catalyst. Although monoliths exhibit high selectivity, the activity is lower than the slurry catalyst because of the external mass transfer resistance. Therefore, the slurry reactor still has better performance than monolithic. Hence, more improvements in structured catalysts need to be developed.

In conclusion, the structured catalyst could be a good way to carry out multiphase reactions. However, improvements in mass transfer must be done to make these reactors more competitive.

1.2. Rotating Foam Reactors

Rotating foam reactors represent another alternative of structured catalyst for multiphase reactions. Solid foams are highly porous materials which consist of a reticulated structure of struts. They have a high area per volume and low pressure drop. The mass transfer in these foams is the main focus of this project. The foams are characterized by the number of pores per linear inch, ppi. The foams can have different geometrical configurations as blades or block to promote the stirring. Figure 1 shows

three different foam materials. More detailed information about the foams used is present in Annex A.

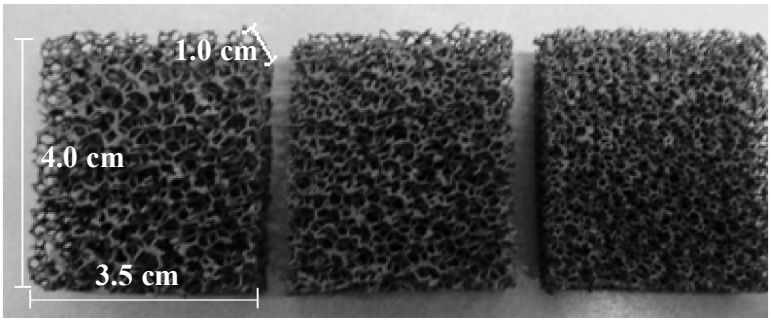

Figure 1: Blades foams used in this project, 10, 20 and 40 ppi, respectively.

In heterogeneously catalyzed gas-liquid reactions, the mass transfer is a combination of three different resistances. Firstly, there is the gas – liquid mass transfer resistance, with the mass transfer coefficient, k_{gl}. Secondly, there is the mass transfer from liquid to the solid, with the mass transfer coefficient, k_{ls}. The last resistance corresponds to the internal mass transfer inside the solid which depends on the diffusion parameter, D_{ef}.

The diffusion parameter just depends on the physical properties of the species involved. On the other hand, the coefficients of mass transfer depend of physical properties and also of the hydrodynamics flows.

Tschentscher et al. [8] studied the gas – liquid mass transfer for rotating foams reactor. They measured the mass transfer coefficient for different stirrer designs like two foam blades or foam block, and compared them with the Rushton stirrer which is normally used in slurry reactors. They concluded that both foam stirrer configurations exhibited a higher mass transfer coefficient than the Rushston turbine for the same stirrer speed, with volumetric gas – liquid mass transfer coefficient between 0.05 and 0.2 s^{-1}. Moreover, they found that the foam block has a slightly higher mass transfer coefficient than the foam blades, for high stirrer speed, above 400 *rpm*.

Tschentscher [9] also studied the liquid – solid mass transfer for a slurry reactor and for a rotating foam block reactor. The dissolution of copper by potassium dichromate was used as a model. They estimated the mass transfer coefficient and the influence of stirring speed on this parameter. For the foam blocks stirrer reactors the value reported for the liquid – solid mass transfer coefficient was about 2.5×10^{-3} $m.s^{-1}$.

This project focuses on liquid – solid mass transfer in rotating foams reactors using a blade stirrer. The main objectives of this work are to study the kinetic of reaction and measure the liquid – solid mass transfer and compare the performance for the different ppi foams.

1.3. Reaction Model

The hydrogenation of styrene over Pd/γ-Al_2O_3 was chosen as a model reaction which is carried out in an autoclave reactor. Styrene is one of the components present in the pyrolysis gasoline. This is an important reaction for the fuels industries. The kinetics for this reaction have been already studied by Cheng et al., Nijhuis et al., and Zhou et al. [10,11,12]. The activation energy was estimated by them around 51, 54 and 27 $kJ.mol^{-1}$, respectively. Nijhuis et al. also modelled the reaction carried out in a monolithic and in a trickle-bed reactor taking in account the mass transfer effects.

Zhou et al. considered the selective adsorption of the different components that are present in the pyrolysis gasoline (PYNGAS) on the catalyst. This improved the kinetics studies because it represents better the real process. Furthermore, they used the Soave – Redlich – Kwong [13] cubic equation in order to estimate the solubility of hydrogen in PYNGAS mixture. The range of temperature and pressure used was 298 – 343 K and 1 – 6 MPa, respectively. They found a Henry constant between 0.055 and 0.068 $mol.L^{-1}.MPa^{-1}$.

1.4. Catalyst Preparation

The foam catalyst based on aluminium foam can be prepared as follows: anodization, wash coating and palladium impregnation.

In the anodization produce a highly stable alumina layer is grown by oxidizing the aluminium struts surface. This step increases the foam surface and improves the anchoring of alumina coating. However, the surface area obtained is still low to be used as catalyst support. The wash coating techniques can be used in order to further increase the surface area. This technique increases the surface area. Finally, the last step is the impregnation of palladium on the support catalyst.

Tschentscher et al. [14] prepared alumina coated monoliths by anodization and wash coating. With the anodization the foam reached a specific area of 2.5 $m^2 \cdot g^{-1}_{foam}$, and the average loss of mass round the 2%. In order to increase the area surface, they applied the wash coating reaching a surface area about 24 $m^2 \cdot g^{-1}_{foam}$.

Tronconi et al. [15] also studied the wash coating technique. They compared different wash coating techniques like the sol-gel dispersion and the slurry method. Both techniques show similar performance in terms of activity and mass transfer resistance. Moreover, they present a technique for the palladium impregnation, using a solution where the mass of palladium dissolved represent 3% of the alumina coating.

The aim of this project is to prepare palladium on alumina coated foam as catalyst for the hydrogenation of styrene and to model the reaction rate taking into account the effect of mass transfer. The influence of the stirring speed and the foam cell density on the reactor performance is studied.

2. Catalyst preparation and characterization

2.1. Catalyst Preparation

As discussed in the introduction, the catalyst preparation involves three steps. The first one is the anodization, follows by the wash coating and the palladium impregnation. The main material of the catalyst support is aluminium foam. Since this material has a low surface area for catalyst deposition, an alumina layer is grown by anodization in order to increase the area. This surface treatment is also applied with the aim of increasing the mechanical anchoring of the washcoating to the support. In the figure below, the scheme of the anodization tank is show.

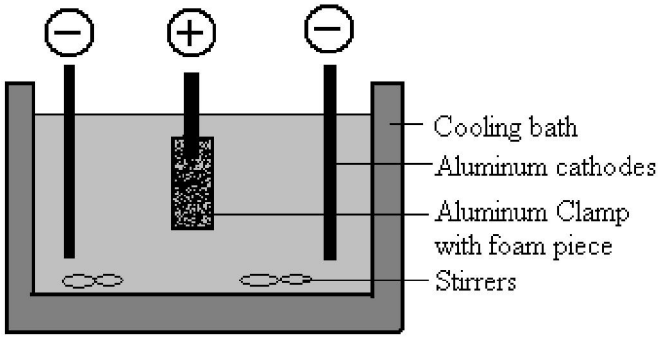

Figure 2: Scheme of the anodization tank

2.1.1. Anodization

The anodization will turn the surface of the aluminium in porous alumina (Al_2O_3), the responsible for the increased porosity and area. For this oxidation a current of 2 $mA.cm^{-2}$ is applied, during 60 *min* at the bath temperature equal to 10^oC. The bath, or the electrolyte, is acid solution with oxalic acid, at 0.08 $mol.L^{-1}$, and phosphoric acid, at 0.5 $mol.L^{-1}$. The negative poles are connected to the aluminium plates, cathodes, and the positive pole is connected to the aluminium clamp which holds the foam, anode.

The electrochemical process involved in this treatment is explained with the following equations. Firstly, water is converted in hydrogen in the cathode phase:

$$6H_2O + 6e^- \rightarrow 6OH^- + 3H_2 \qquad (2.1)$$

At same time the aluminium is oxidized, and dissolved at the metal-oxide interface of the anode:

$$2Al \rightarrow 2Al^{3+} + 6e^{-} \quad (2.2)$$

Lastly, the cations react with OH^{-} to form alumina layer:

$$2Al^{3+} + 6OH^{-} \rightarrow 2Al_2O_3 + 3H_2O \quad (2.3)$$

The choice of operating conditions influences strongly the morphology of the oxide layer. The conditions used in this experiment were defined by comparing the work realized by Tschentscher et al. [14] and Sanz et al. [16,17]. Sanz et al. compared the influence of different parameters, as time, temperature, acid concentration and current density, on the final surface morphology. Furthermore, this study was done on foam and monoliths, and they concluded that each parameter have a critical value which promotes the cracking surface.

2.1.2. Washcoating

After the anodization, the washcoating is used in order to increase the surface area. In this step, the foam structure reaches the required area to be used as a catalyst support. Summarizing, the washcoating is the deposition of a catalyst support material layer on the foam structure, followed by calcination, where the washcoat becomes stable. In the present project, the slurry washcoating method was used for alumina washcoating.

Firstly, in order to prepare the slurry solution, the alumina particles, with an average diameter of 108.5 μm, was mixed with water in half to half proportion followed by ball-milling for 24 hours. This step is done to decrease the particle diameter in order to ensure stable slurry for washcoating and to create a homogeneous alumina layer. After, the mixture is dried at 120ºC. The slurry solution is composed by 65%wt of water, 20%wt of alumina and 15% wt of colloidal boehmite, the last one is used as binder. To guarantee homogenous suspension, the adding of alumina must be done slowly and the pH should be kept at 7 for avoiding the particle agglomeration. For this purpose, some dropper of acid nitric could be added to the solution to keep the desired pH.

Afterwards, the foam is immersed on the slurry solution during one minute. The excess of alumina is removed by pressurized air and followed by drying at room temperature for 3 hours. During this time the foam is rotating at slow stirrer speed in order to make a homogeneous coating. After this procedure the foam is calcined at 550ºC, for 4 hours, to ensure the stability and adhesion of the coating. Finally, the foam is submerged in a water tank, at high stirrer speed to eliminate the alumina that is not strongly adhered to the surface, and dried over night at 120ºC.

2.1.3. Palladium impregnation

Palladium impregnation is the last process of the catalyst preparation. In this step the foam becomes active for the hydrogenation reaction. In order to impregnate the foam with palladium, a solution of palladium acetate, $Pd(OAc)_2$, is prepared with the desired amount of palladium diluted in toluene. Then, the foam is immersed on the solution for 24 hours with stirring. In this project 3%wt of palladium loading was used which corresponds to the washcoating mass deposited on the foam.

After, the foam is calcined at 300ºC for 4 hours and reduced by a sodium borohydride solution at room temperature (20 *ºC*). The solution used in the present work was composed by 50 times more moles of sodium borohydride than the moles palladium impregnated.

2.2. Results and Discussion

In the present work, foam of different ppi, 10, 20 and 40, are used for the styrene hydrogenation. As explained in the catalyst preparation sub-chapter, three processes were used in order to increase the surface area and to activate the foam.

2.2.1. Washcoating Results

In Figure 3 the alumina loading for the different ppi foam is showed. The values correspond to the average loading on different foams with the same ppi. As shown in the graph, there is a slight increase in the alumina loading of 10 ± 3% to 15 ± 3% when compared the 10 ppi foams with the 20 ppi foams. However, for the 40 ppi foams the loading increased significantly, reaching 66 ± 20 in mass.

This increase of alumina loading with the increase of ppi number was expected due to the consequently increase area per volume. For the different ppi foams used, 10, 20 and 40, the area per volume of foam is 800, 1700, and 2700, respectively. However, the extreme increase for the 40 ppi foams is also due to large number of struts on the foam. The most part of alumina coating is accumulated in the corners of the struts.

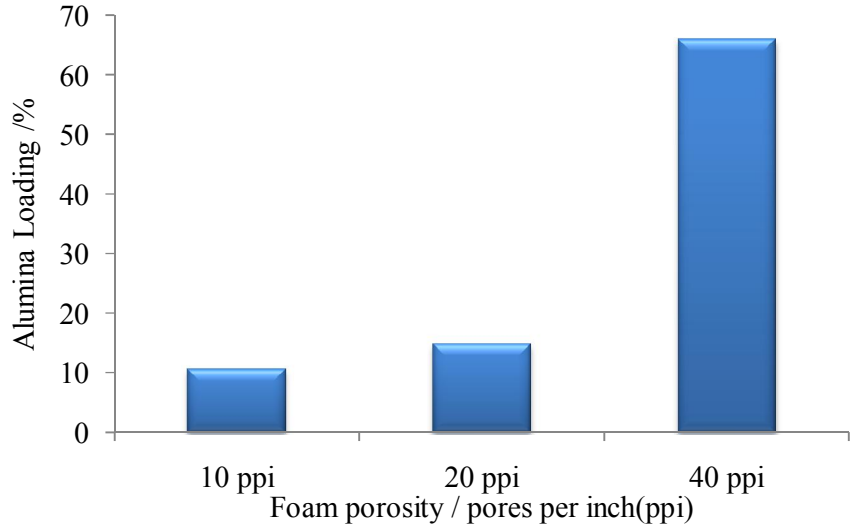

Figure 3: Comparison of percentage of alumina loading, per mass of foam, by wash coating with just one layer, for different porosity foam.

In order to study the influence of the thickness layer on internal mass transfer resistance, 2 and 3 washcoat layers were deposited on the same ppi foam. Figure 4 shows the average percentage of alumina loading for one, two and three washcoating. As expected, it can be seen that the alumina loading increases with the number of washcoating applied.

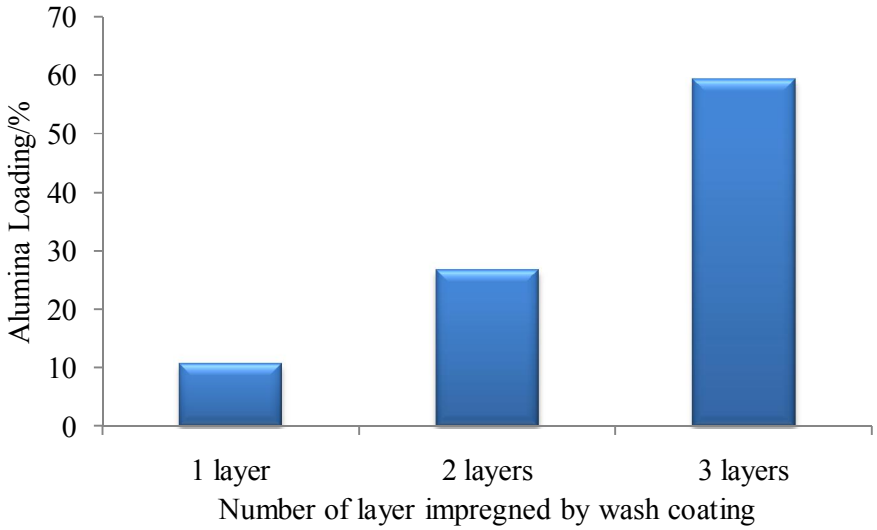

Figure 4: Comparison of percentage of alumina loading in washcoating, per mass of foam, on 10 ppi foam, for different wash coating times.

The amount of alumina deposited on the foam allows estimating the average thickness of the coating. For that purpose, a homogeneous coating was considered. The average thickness was calculated considering that the alumina coated have the same thickness over whole the surface area.

Figure 5 shows the average thickness for the different configurations of foam used. The average thickness estimated increases more with application of more alumina layers than when increasing the foam ppi. This can be explained by the simultaneous increase of the alumina loading and surface area with the increase of the foam ppi. Furthermore, this slightly increase of thickness with the foam ppi prove the previous affirmation, that there are more accumulation on the corner struts. However, the same thickness would be expected. The difference between the average thickness estimated by the mass of alumina loaded and the observed by SEM is due to the low number of observed points in SEM, because the thickness depends of spot in the structure, near of the corners more accumulation is observed.

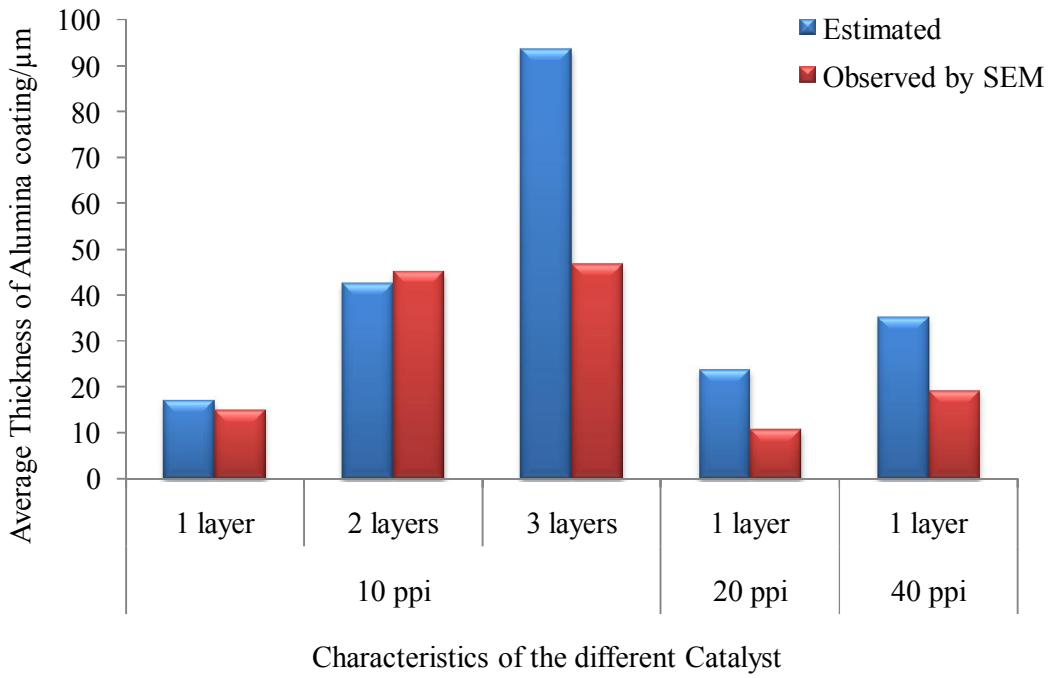

Figure 5: Average thickness of alumina layer for the different catalyst used on the experiments, foam porosity and number of wash coating layers, estimated and observed by SEM.

As mentioned before, the average thickness was estimated by considering a homogeneous distribution of the alumina on the foam surface. This estimative represents an ideal situation, which is different from the reality. However, the average thickness estimated is approximately in the same range as the ones observed by SEM.

Therefore, the estimated thickness can be used for modelling the reaction and the reactor performance. Figures 6 - 10 show that there are some parts of the foam in which the thickness measured by SEM is higher than the average thickness estimated. This confirms that the accumulation of alumina in the foam corner struts is an issue. This situation can be well observed in the first image of Figure 8, where the corner strut can be observed and the measured thickness was bigger than the estimated.

Therefore, the estimated thickness can be used for modelling the reaction and the reactor performance, once the estimated value is supported by the results of SEM images.

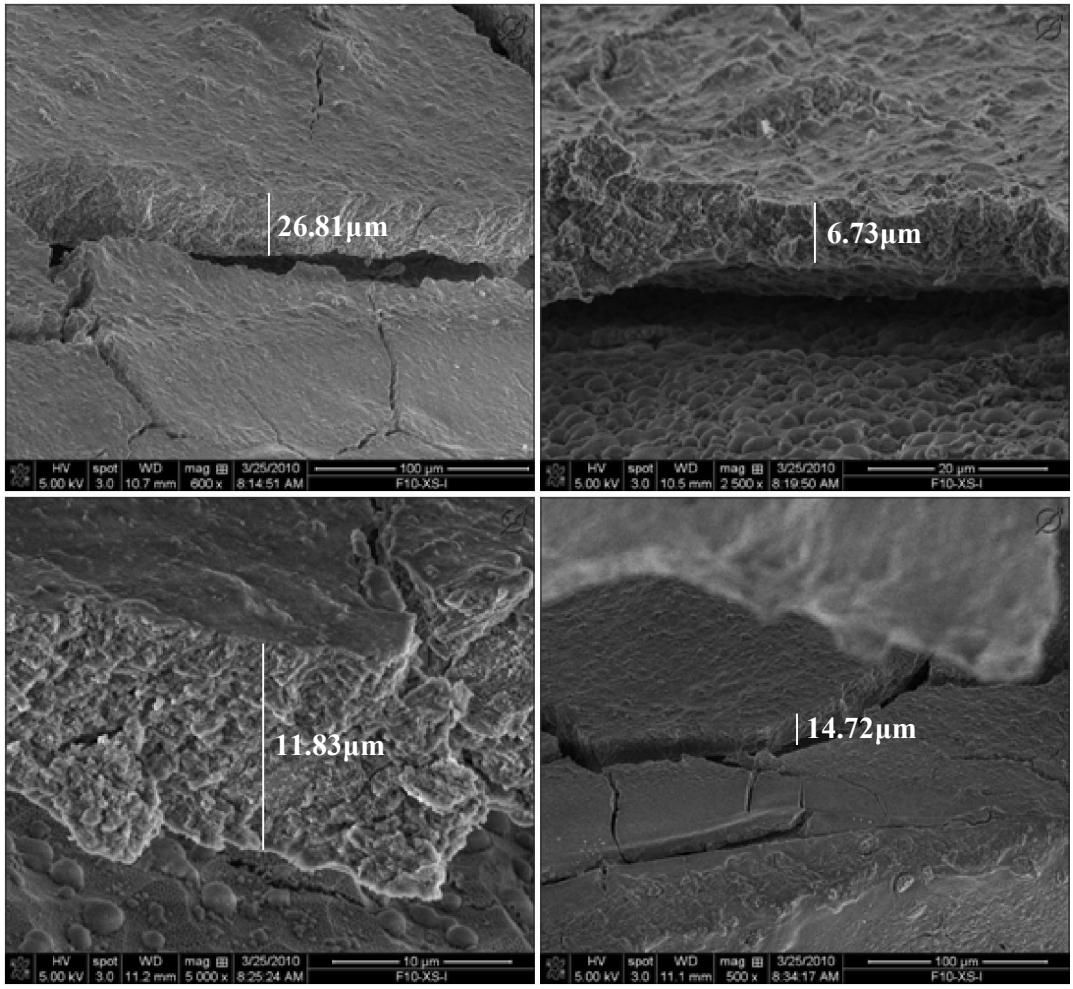

Figure 6: Images of alumina layer on the anodized foam, captured by SEM, for the 10 ppi foam and 1 alumina layer.

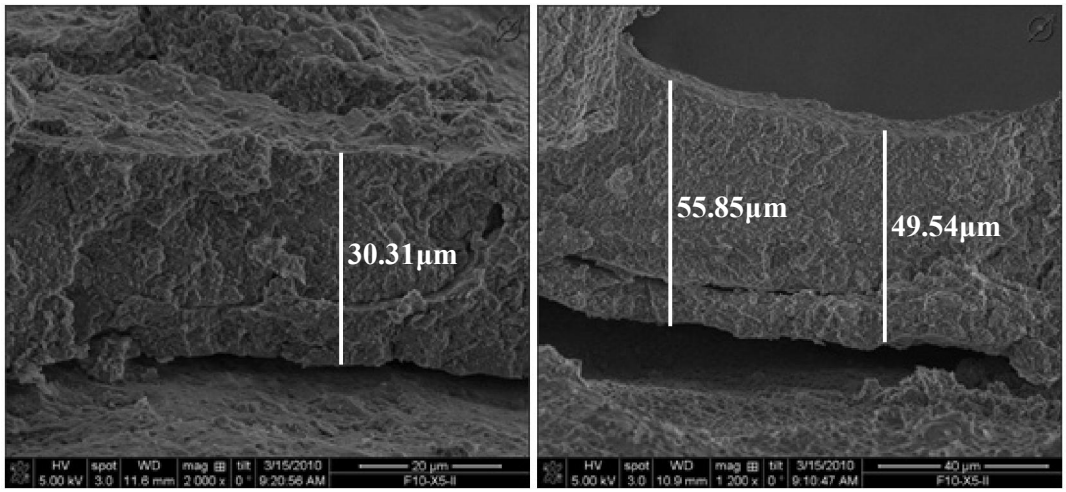

Figure 7: Images of alumina layer on the anodized foam, captured by SEM, for the 10 ppi foam and 2 alumina layer.

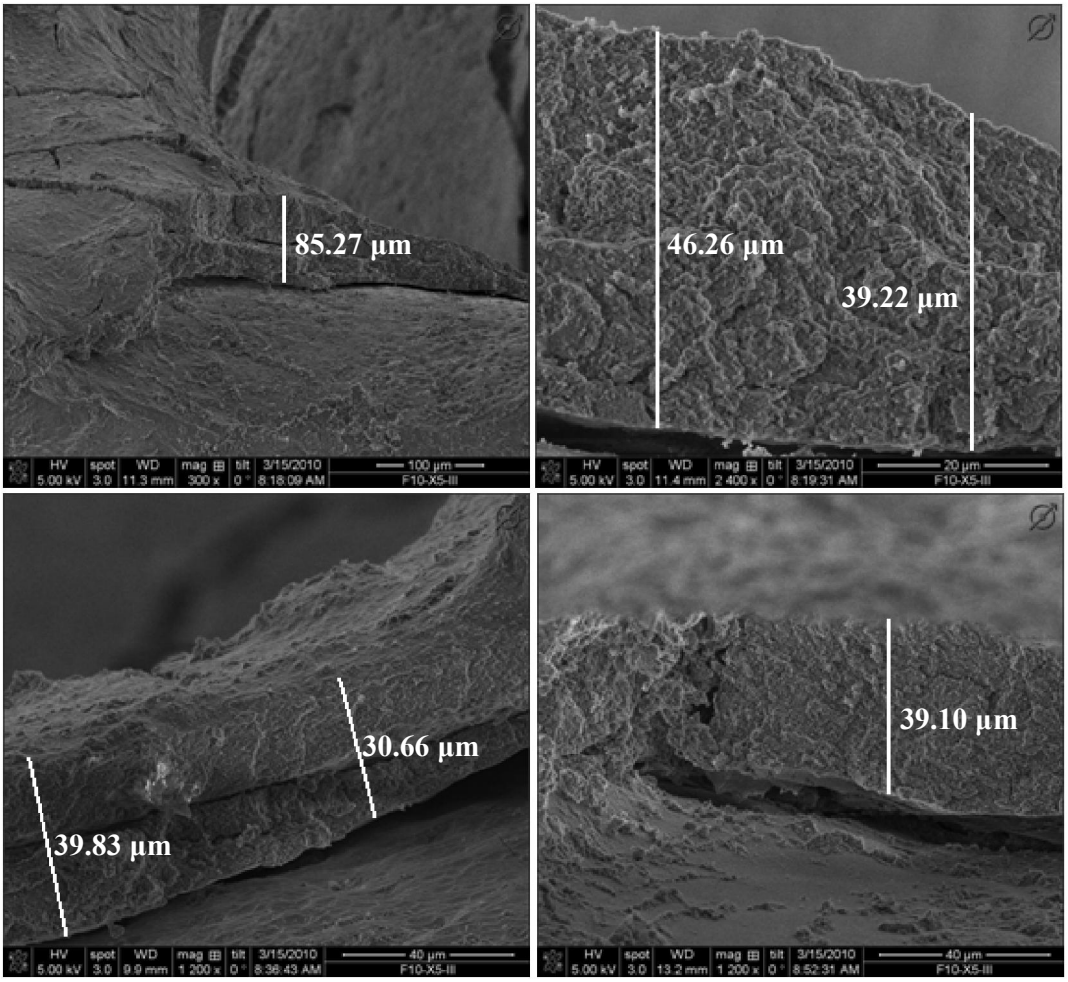

Figure 8: Images of alumina layer on the anodized foam, captured by SEM, for the 10 ppi foam and 3 alumina layer.

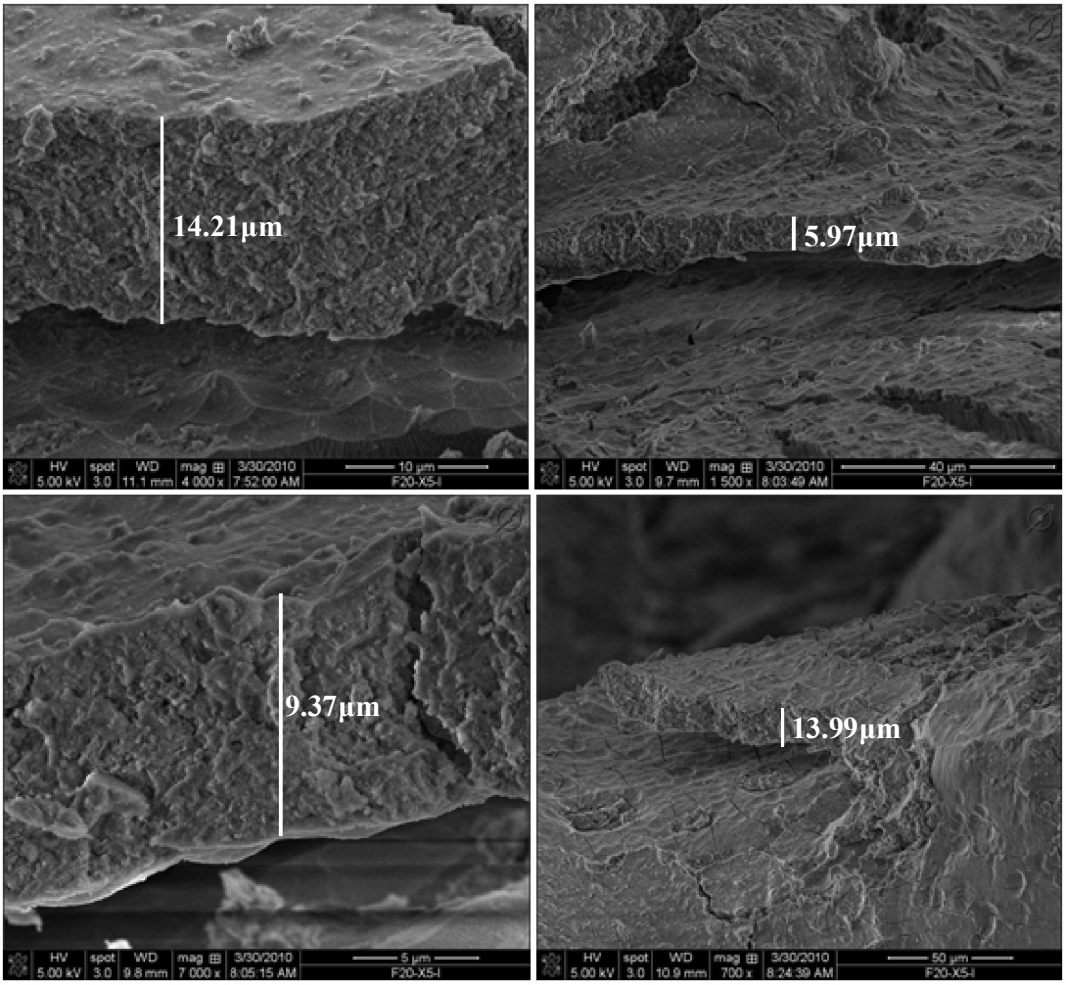

Figure 9: Images of alumina layer on the anodized foam, captured by SEM, for the 20 ppi foam and 1 alumina layer.

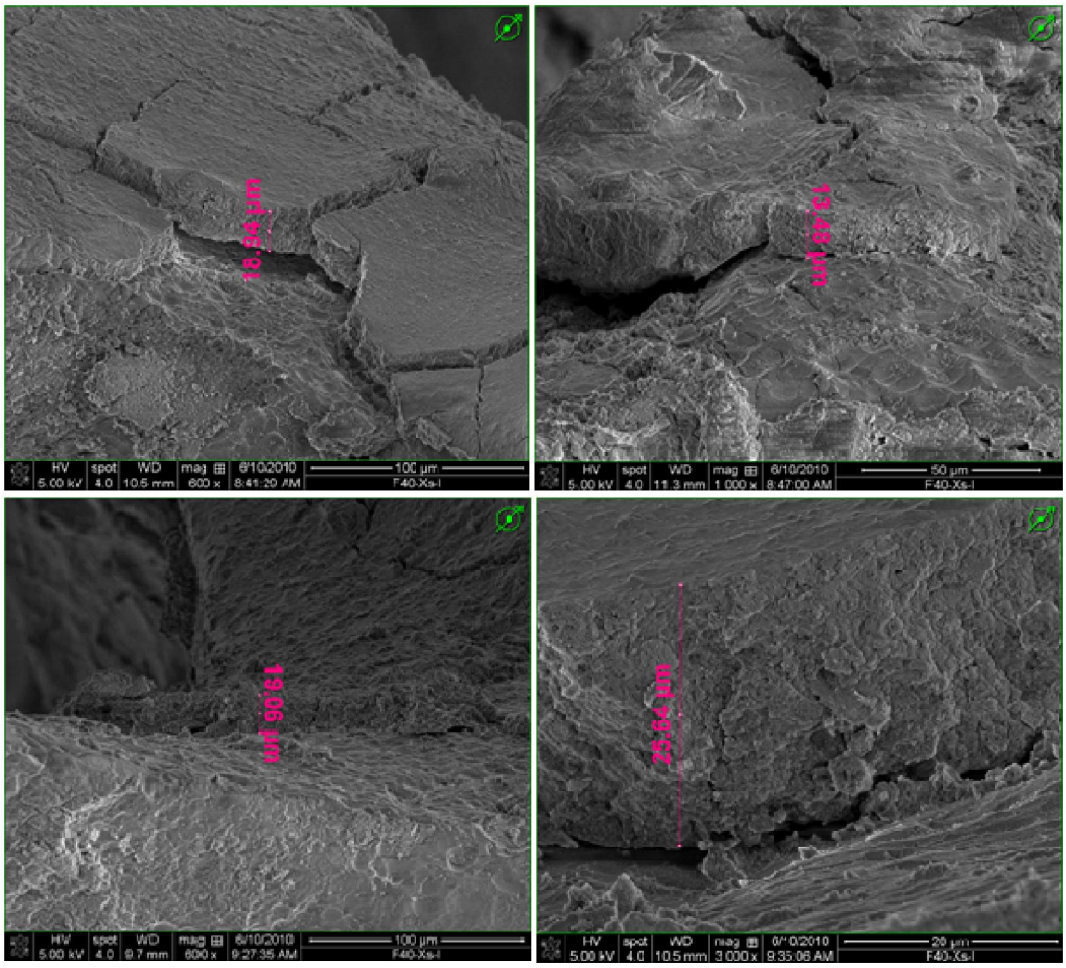

Figure 10: Images of alumina layer on the anodized foam, captured by SEM, for the 40 ppi foam and 1 alumina layer.

2.2.2. Palladium impregnation results

After palladium impregnation, on the washcoating surface, Transmission Electron Microscopy (TEM) was used in order to characterise the dispersion and the diameter of palladium particles. The results obtained by TEM shows a good dispersion of palladium and a narrow distribution of particles diameter for the different foams density cell, 10, 20 and 40 ppi.

The figure below was taken for 10 ppi foam. A homogeneous particles distribution can be observed. The darkness points on the picture represent the palladium particles.

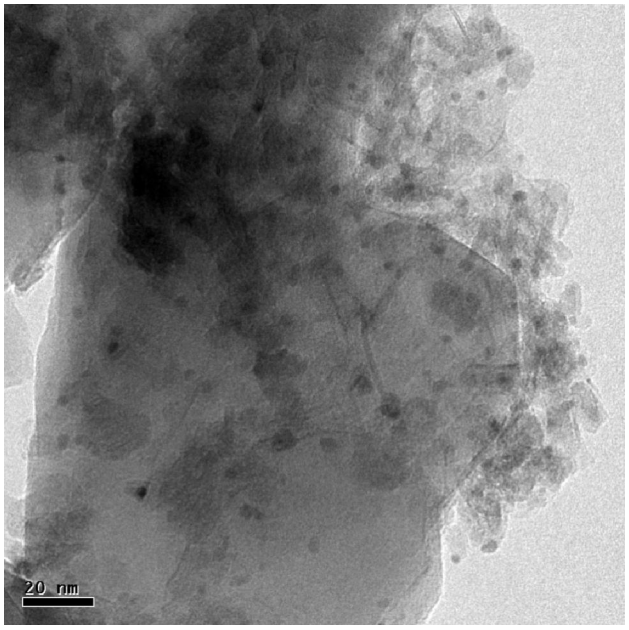

Figure 11: Image captured by TEM from 10 ppi foam, after palladium impregnation.

The particles size distribution curve can be obtained from the TEM images by direct diameters measurements. Therefore, analyse of several images allowed to estimate the diameter distribution. Figure 12 shows the distribution of Palladium particles. Moreover, an approach of narrow distribution can be observed, with an average diameter of 2.2 ± 0.5 μm, in a total of 115 observed points.

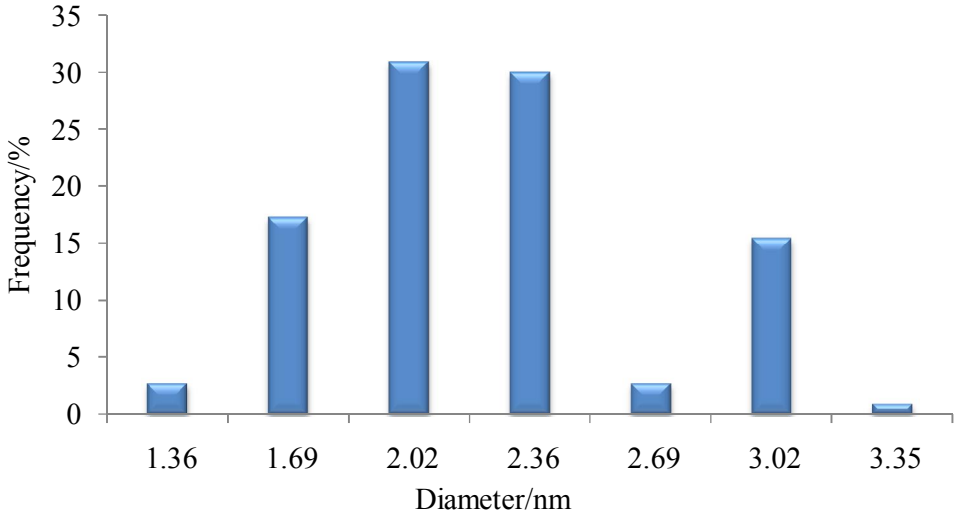

Figure 12: Distribution of particles diameter, of palladium, for 10 ppi foam.

Also for 20 ppi foams, the homogeneous particles distribution is observed. Figure 13 is one of the images captured by TEM. As the picture shows, there is a good distribution of the palladium on the alumina coating.

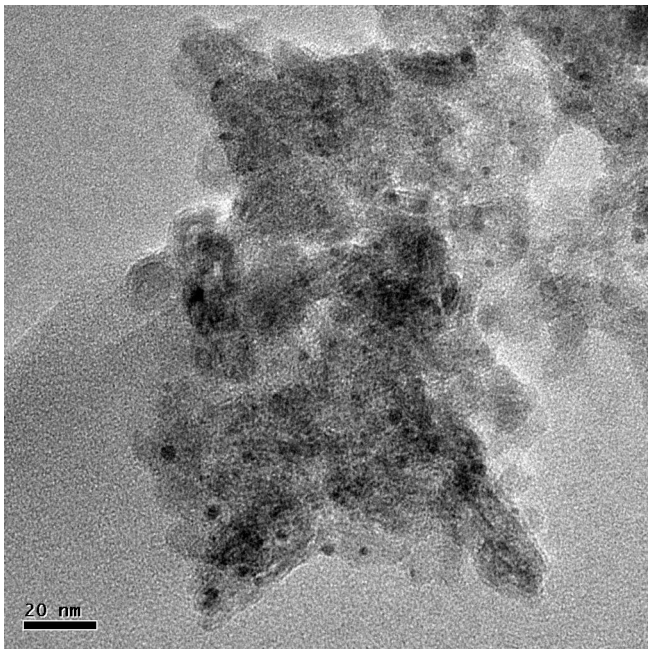

Figure 13: Image captured by TEM from 20 ppi foam, after palladium impregnation.

With all images obtained by TEM images Figure 14 was plot, which represents this diameter distribution, for 20 ppi foam, with total of 90 observed points. It can be seen that the graphs shape approach to a narrow distribution, with an average diameter equal 2.2 ± 0.7 *nm*.

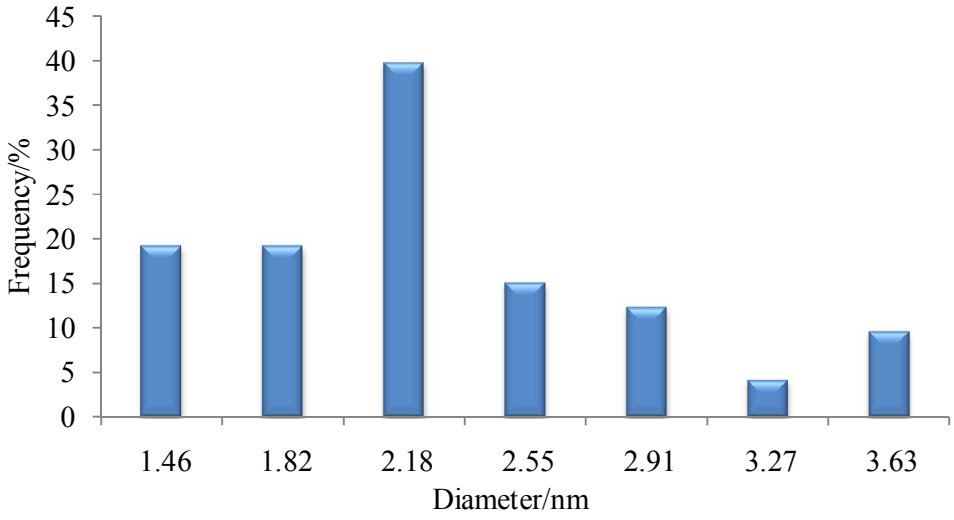

Figure 14: Distribution of particles diameter, of palladium, for 20 ppi foam.

For the 40 ppi foams, a homogeneous distribution was also observed by TEM. This can be observed on Figure 15. Furthermore, a narrow distribution of the size was also observed by the measurement of particles diameter, and an average diameter of 2.2 ± 0.6 *nm* was estimated. The diameter distribution is represented on Figure 16 with 184 measured points.

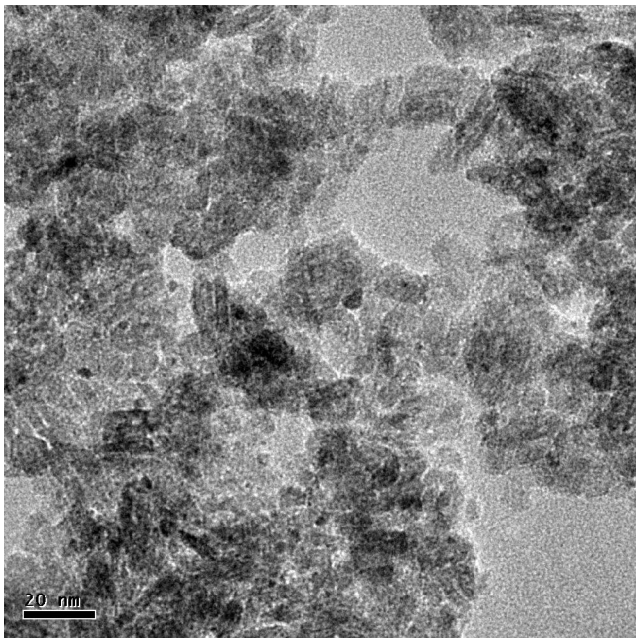

Figure 15: Image captured by TEM from 40 ppi foam, after palladium impregnation.

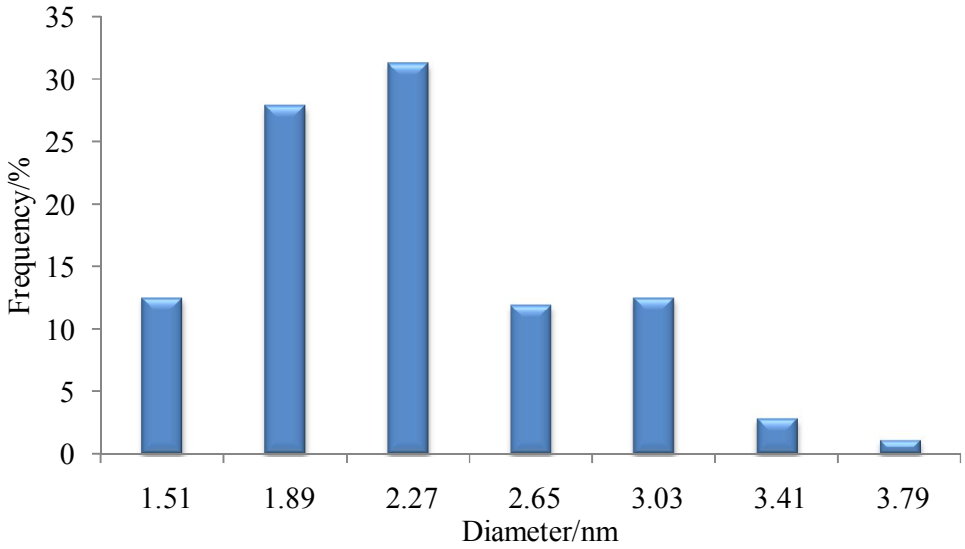

Figure 16: Distribution of particles diameter, of palladium, for 40 ppi foam.

In conclusion, a homogeneous distribution of the Palladium particles was obtained for the different ppi foams when using the ion exchange method for palladium impregnation. The ppi number didn't influence the palladium dispersion on the palladium particle size.

The average particle diameter estimated for the three different ppi foams was 2.2 *nm*. This can be explained by the amount of Palladium impregnated. If the amount of palladium added were the same for the 10, 20 and 40 ppi foams, a different mean diameter was expected due to the difference in surface area, lower for the bigger ppi number.

However, the amount added is proportional to the mass of alumina coating, and consequently leads to the similar average diameter.

3. Reactions

3.1. Start up Reaction

The start up process is an important step for the hydrogenation of the styrene since this is a monomer that can polymerize itself in the presence of light or at high temperatures. For avoiding polymerization during storage, the supplier adds an inhibitor to the styrene. The tert-butlycatechol is the inhibitor used.

However, this inhibitor also decreases the rate of hydrogenation of styrene due to the adsorption competition on the catalyst. Furthermore, the regeneration of the catalyst is not always efficient. The figure below shows the performance of a fresh catalyst with two different regeneration methods. In first method, the foam was washed with toluene and dried overnight at 120ºC. The second method consists in heating the foam after washed with toluene for four hours at 300ºC, the calcination temperature, followed by the reduction with $NaBH_4$. Figure 17 shows that no big difference can be observed between the two regeneration methods. However, there is a large difference between the activity of the used and the fresh catalyst that can be explained by the irreversible adsorption of the inhibitor.

The second regeneration method was defined by taking into account two works performed for the regeneration of similar catalyst when poisoned by thiophene. Those two papers [18,19] studied the deactivation of the palladium catalyst by thiophene and also the procedure to regenerate the catalyst. The catalyst regeneration consisted of exposing the catalyst at high temperature and hydrogen pressure. The high temperatures are used to promote desorption of the sulphur, and the hydrogen is used to reduce the palladium again.

However, they could just remove part of the sulphur since other part was still adsorbed irreversibly on the catalyst surface. Although the increase of temperature leads to higher sulphur removal and therefore to an increase of the catalyst activity, the temperature cannot be very high, otherwise catalyst sintering can occur.

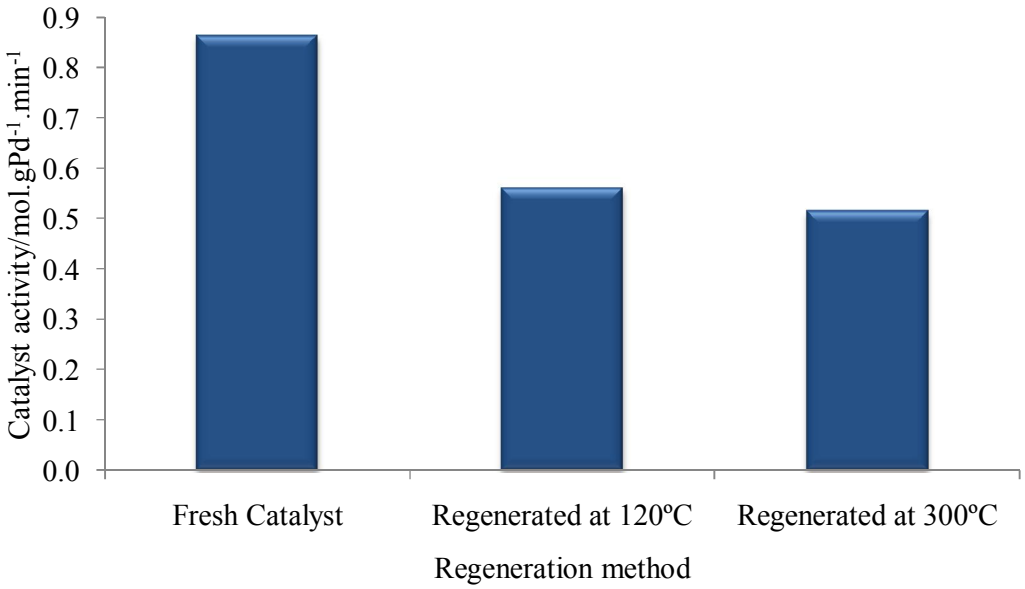

Figure 17: Catalyst activity, using 20 ppi foam, at 40ºC, 800 rpm and 15 bar of hydrogen pressure, and comparing the performance of two different regeneration methods with the fresh catalyst in the presence of inhibitor.

Therefore, in order to increase the reaction rate and avoid the catalyst poisoning the tert-butlycatechol is removed. This can be done by a distillation batch since the normal boiling point of two components are very different, 283ºC and 145ºC for the tert-butlycatechol and styrene, respectively. However, a vacuum distillation must be used to avoid high temperatures and the consequently polymerization of styrene. Therefore, the boiling point of styrene in vacuum distillation decreases to 52ºC. After distillation, the styrene without inhibitor is stored at -18ºC.

The reaction starts up with the pre-heating of the solvent, toluene, and hydrogen, in the presence of the catalyst, to the desired temperature. When the desired temperature is reached and the other parameters, like hydrogen pressure and stirrer speed, are stable at their set points, the styrene is added to start the reaction.

Although the polymerization of styrene is not very fast below 90ºC [20], this procedure will avoid the polymerization of the styrene and consequently prevent a possible deactivation of the catalyst. Figure 18 shows the catalyst activity when the catalyst is fresh and when it has been used two or three times. In all cases, the catalyst was regenerated by washing the foam with Toluene and drying overnight at 120ºC.

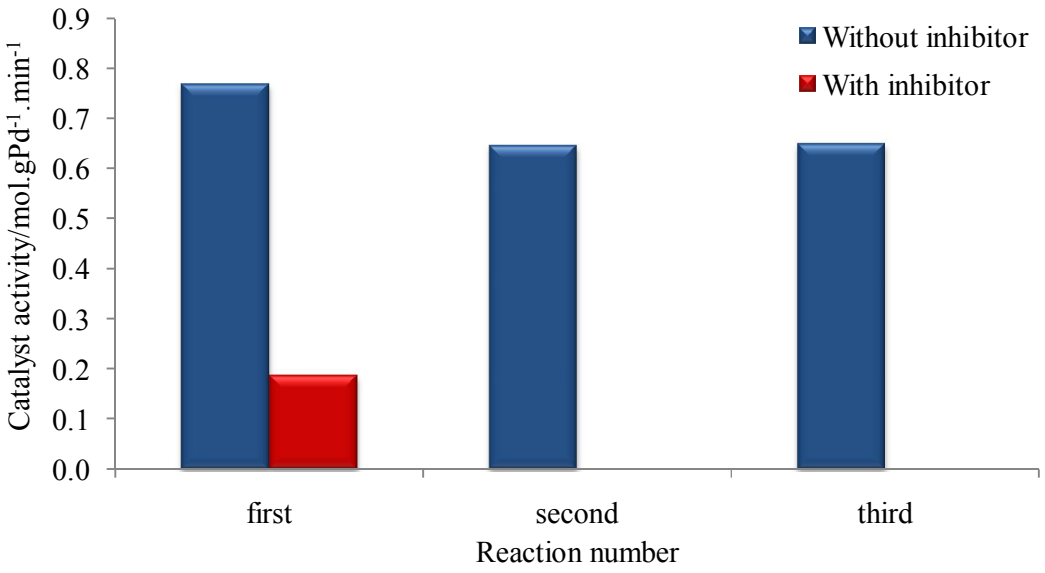

Figure 18: Catalyst activity for the reaction using an 40 ppi foam, at 40ºC, 800 rpm, and 15 bar of hydrogen pressure, by regenerate the catalyst at 120ºC overnight. With and without inhibitor.

Figure 18 shows that a slightly deactivation can be observed between the first and the second reaction. However, the activity remains constant after the second reaction. This can be caused to the high stirring speed used during the reaction that removes some catalyst from the foam that it is not well adherent. This is similar to the test used for measuring the washcoat stability. Furthermore, the graph also shows the difference between the catalyst activity for the reaction with and without inhibitor. The reaction is four times faster without inhibitor.

3.2. Mass transfer and kinetic regimes – operation condition range

In addition to define the start up of reaction, the operation conditions for the different mass transfer and kinetic regimens must be also defined. Therefore, the influence of temperature on the apparent activation energy was study in order to distinguish kinetic, internal mass transfer and external mass transfer regime.

According to J. Weitcamp [21] and other authors, the apparent activation energy is half of the real activation energy for internal mass transfer regime and less than 5% for external mass transfer regime.

3.2.1. Kinetic Regime Parameters

Figure 19 shows the influence of the temperature on the initial reaction rate. It can be seen that above 50ºC ($3.1x10^{-3}\ K^{-1}$) the temperature does not have any influence on the initial reaction rate. Therefore, it can be concluded that internal mass transfer limitations were negligible and external mass transfer controls the overall reaction rate.

For the last 3 points corresponding to 25ºC, 30ºC and 35ºC, a linear behaviour can be observed. The apparent activation energy can be estimated by the slope of this straight line, assuming the Arrhenius equation for the kinetic constant rate:

$$k = k_0 e^{-\frac{Ea}{R.T}} \qquad (3.1)$$

Where k is the kinetic constant rate, k_0 represent the pre-exponential factor, Ea the activation energy, R the ideal gas constant and T the absolute temperature.

The activation energy estimated was 54 $kJ.mol^{-1}$. This value is similar to the value reported by others authors for the real activation energy. X. Nijhuis et al. (2003) [11] estimated 54 $kJ.mol^{-1}$, S. Jackson and D. Shaw (1996) [22] reported 41 $kJ.mol^{-1}$ and R. Chaudhari et al. (1986) [23] estimated 55 $kJ.mol^{-1}$. Assuming that those authors have estimated the real activation energy it can be concluded that kinetic controls the overall reaction rate at temperatures below 35ºC.

However, other authors as Z. Zhou et al. (2006) [12] and Y. Cheng et al. [10] have reported 26 and 15 $kJ.mol^{-1}$ for the activation energy, respectively. Those values are very low when comparing with the other authors. This can be explained by internal mass transfer, and therefore they were not estimated in real kinetic regime.

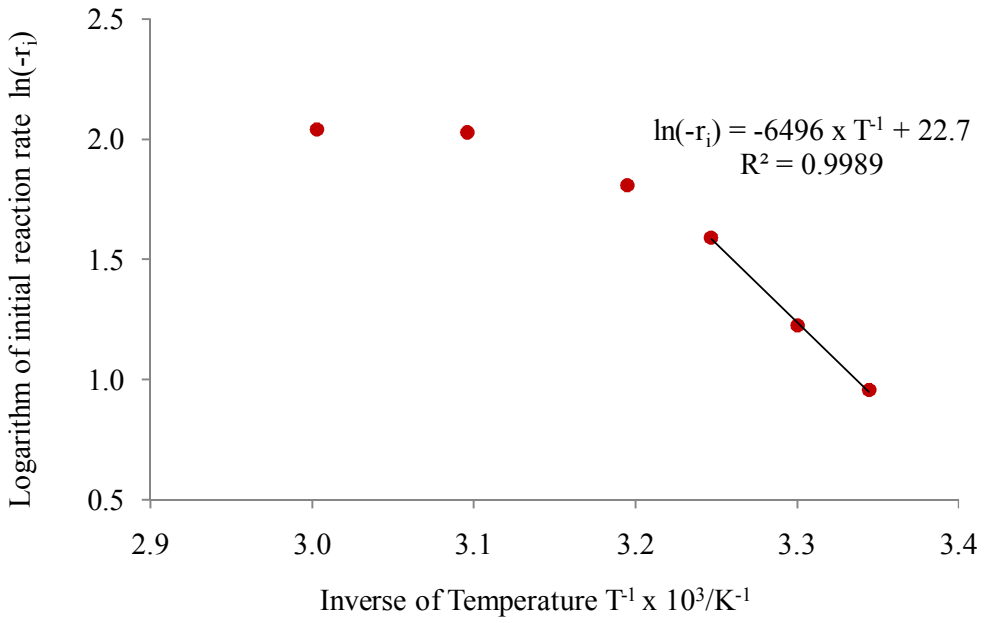

Figure 19: Logarithm of initial rate**,** k ($mol.m^{-3}.min^{-1}$) versus the inverse of the Temperature, at 725 rpm, hydrogen pressure of 15 *bars*, Styrene initial concentration of 650 $mol.m^{-3}$, with a palladium mass of 18.8 *mg* at 2.8 $mg_{Pd}.g_{foam}^{-1}$.

The kinetic of this reaction catalyzed by palladium follows the Langmuir equation as Nijhuis et al. [10] have reported. The kinetic rate expression is shown below.

$$(-r_i) = W_{Cat}.k.C_H \frac{K_{Sty}.C_{Sty}}{1 + K_{Sty}.C_{Sty}}, \text{where } i = [Sty, H] \quad (3.2)$$

Where C_H and C_{Sty} are the concentration of Hydrogen dissolved in the liquid and Styrene, respectively. K_{Sty} is the adsorption equilibrium constant of Styrene, W_{Cat} is the mass of palladium in the reactor and $(-r_i)$ is the reaction rate.

The pre-exponetial factor, k_0, was estimated using the kinetic equation and the data collected in the kinetic regime. The value estimated by the experimental data was 6.22 x 10^9 $g_{Pd}^{-1}.min^{-1}$.

3.2.2. External Mass Transfer: Gas – Liquid versus Liquid – Solid.

In order to identify which of the external mass transfer resistances, liquid – solid, gas – liquid or both, is controlling the reaction rate, the reaction was performed with one and two actives blades. The characteristics of the actives foams used are present in Annex A.

The liquid - solid mass transfer rate is directly proportional to the increase of area surface, proportional to the number of active blade. For liquid – solid mass transfer regime, the increase of solid surface area leads to the same increase of reaction rate or activity, since the mass transfer is directly proportional to the transfer interfacial area.

For the gas – liquid mass transfer regime, an increase of active blade does not influence the hydrodynamic of gas – liquid mixing. Therefore, no change in reaction rate is expected for this regime.

In the case that both external mass transfer regimes, gas – liquid and liquid – solid, are influencing the overall reaction rate, the increase of activity or reaction rate will be proportional to the percentage of the relative percentage of controlling of liquid –solid mass transfer.

Thus, two reactions were carried out with different number of active blades, one and two, and the results regarding the catalyst activity were compared. The main reaction conditions are described in the following table.

Table 1: Operation conditions of reaction, for external mass transfer study

	Reaction 1	Reaction 2
Temperature T / *K*	333	333
Hydrogen pressure P_H / *bar*	15	15
Catalyst concentration C_{cat} / $mg_{Pd}.L^{-1}$	12	11
Number of actives blades	2	1
Stirrer speed / *rpm*	350	350
Foams used	F_{10}-X_8 and F_{10} – X_9	F_{10}-X_{10}
Catalytic area per liquid volume a_{LS} / $m_{LS}^2.m_L^{-3}$	18.6	9.9

Those operation conditions showed in Table 1 are the same used for the parameter estimation towards external mass transfer regimes, the mass transfer coefficients. The catalyst concentration is a little bit different for both reactions, however, no activity change is expected due to kinetic term, since the temperature is too high and mass transfer is controlling the reaction.

The activity obtained is reported in the next table as well as the total transfer area ratio for the two systems.

Table 2: Comparison between reaction activity and liquid-solid surface area

	Area per volume of liquid ratio - a	Activity / $mol.g_{Pd}^{-1}.min^{-1}$	Activity ratio - b	Relative difference a-b
Reaction 1	1.88	0.337	1.83	2.5 %
Reaction 2		0.184		

As it can be observed in the table above, there is a small difference between the activity ratio and the surface area ratio, 2.5%. Therefore, it can be considered that there is no gas – liquid mass transfer resistance, which makes the reactor modelling more straightforward. This proves that the liquid – solid mass transfer is controlling the overall reaction rate at 60 *ºC*.

3.2.3. Internal Mass Transfer: Effectiveness estimation

For studying the internal mass transfer, the estimation of diffusion coefficient for both reactants is needed. Wilke and Chang [24] developed a correlation to estimate the diffusion coefficient of a gas (1) dissolved in a liquid (2).

$$D_{12} = \frac{1.1728x10^{-16}(\theta_2 M_2)^{1/2}T}{\mu_2 V_{m1}^{0.6}}, m^2 s^{-1} \quad (3.3)$$

Where D_{12} is the diffusion coefficient of solute (1) in solvent (2), θ is a parameter associated to the solvent, M is the mass molar, $kg.kmol^{-1}$, μ is the viscosity, $Pa.s$ and V_m is the solute molar volume at the normal boiling point, m^3kmol^{-1}. For toluene the associate parameter takes the value of one.

In order to predict the diffusion of styrene in toluene the King et al. [24] method was used:

$$D_{12} = 4.4x10^{-15}\frac{T}{\mu_2}\left(\frac{V_{m2}}{V_{m1}}\right)^{1/2}\left(\frac{\lambda_2}{\lambda_1}\right)^{1/2}, m^2s^{-1} \quad (3.4)$$

Where D_{12} is the diffusion coefficient of solute (1) in solvent (2), μ is the viscosity, *Pa.s*, *Vm* is the solute molar mass at the normal boiling point and λ is the latent heat at the normal boiling point.

Most of those parameters were found in Perry's Chemical Handbook [24]. The correlation developed by Sengers et al. and Kestin et al. [25] for predicting the viscosity of Toluene at different temperatures was used:

$$ln(\mu^*) = -5.2203 + \frac{8.964}{T^*} - \frac{5.834}{T^{*2}} + \frac{2.089}{T^{*3}} \quad (3.5)$$

Where, $T^* = \frac{T}{298\ .15}, \mu^* = \frac{\mu\ (T)}{\mu(T^*)}$ and for $\eta\ (298.15) = 554\ \mu Pa.s$

Once the diffusion coefficients of the reactants in toluene were estimated, the effectiveness factor could be calculated.

For the effectiveness factor estimation, the catalyst pores were considered as plates. This can be estimated by the follow equation:

$$\eta_i = \frac{\tanh\ (\phi_i)}{\phi_i} \quad (3.6)$$

Where η represents the effectiveness factor for component *i* (styrene or hydrogen) and ϕ represents the Thiele Module for each component and could be calculated by the general equation from Levenspiel [26].

$$\phi_i = L.\sqrt{\frac{(-r_i)}{C_i^s D_{eff}^i}} \quad (3.7)$$

Where *L* corresponds to the alumina thickness layer on the catalyst, *m,* C_i^s is the concentration at solid surface for each component and D_{eff}^i is the effectiveness diffusion coefficient that depends on the structure of the catalyst, $m^2.s^{-1}$.

$$D_{eff}^i = \frac{D_i.\varepsilon_{cat}}{\tau} \quad (3.8)$$

Where ε_{cat} corresponds to the catalyst porosity and τ represent the tortuosity parameter.

With those equations and correlations, the effectiveness factor was estimated. In Table 3 the conditions and assumptions used are presented. The values of thickness layers and tortuosity assumed were over estimated. The typical values of tortuosity are around 3 and the foams used on experiments have a thickness layer lower than 40 μm.

Table 4 presents the results of the estimation of diffusion coefficient for hydrogen and styrene as well as their catalyst effectiveness factor. As it can be seen, the effectiveness factor for both hydrogen and styrene are high, almost 100%. It should be remarked that the alumina thickness layer and the catalyst mass (palladium) used were those corresponding to the worst situation of operating condition. The temperature chosen corresponds to the temperature of the experimental condition to determine the external mass transfer.

Therefore, no internal mass transfer resistance are expected under the conditions chosen. As a result, the reactor modelling just includes the liquid – solid mass transfer and the kinetic effects. This model is straightforward and the parameters involved can be easily estimated. Once, that some parameters were overestimated, for the real condition the internal mass transfer is even faster.

Table 3: Considerations to predict the effectiveness factor

Alumina thickness layer L / μm	50
Temperature T / K	333
Initial Styrene concentration C^0_{Sty} / $mol.m^{-3}$	650
Hydrogen concentration in bulk C^b_H / $mol.m^{-3}$	45
Catalyst porosity ε_{cat}	0.4
Tortuosity τ	6
Palladium mass m_{cat} / mg	35

Table 4: Estimation of internal mass transfer parameters

	Styrene	Hydrogen
Diffusion Coefficient $D_{i/Toluene}$ / $m^2.s^{-1}$	3.84×10^{-9}	1.92×10^{-8}
Effectiveness Diffusion Coefficient $D_{i/Toluene}$ / $m^2.s^{-1}$	2.56×10^{-10}	1.28×10^{-9}
Thiele's Module ϕ_i	0.15	0.32
Effectiveness factor η_i	0.99	0.97

3.3. Reactor Model

As it was said before, the hydrogenation of styrene catalysed by palladium was used as model reaction for the mass transfer study on foam catalyst. The hydrogenation of styrene is one to one stoichiometry reaction:

$H_2\,(g) + C_8H_8\,(liq.) \rightarrow C_8H_{10}\,(liq.)$

The reaction is carry out in a batch reactor, the figure below shows the schema of the reactor used. The gas bubbles, the bulk liquid, the catalyst porosity and the catalyst surface were considered for the modelling. The mass balances in the bulk liquid phase was done by taking into account the hydrogen that comes from the gas phase and the flow of both, hydrogen and styrene, to the catalyst surface. As showed before, in the operation conditions used, the overall reaction rate is controlled by the kinetic and liquid – solid mass transfer.

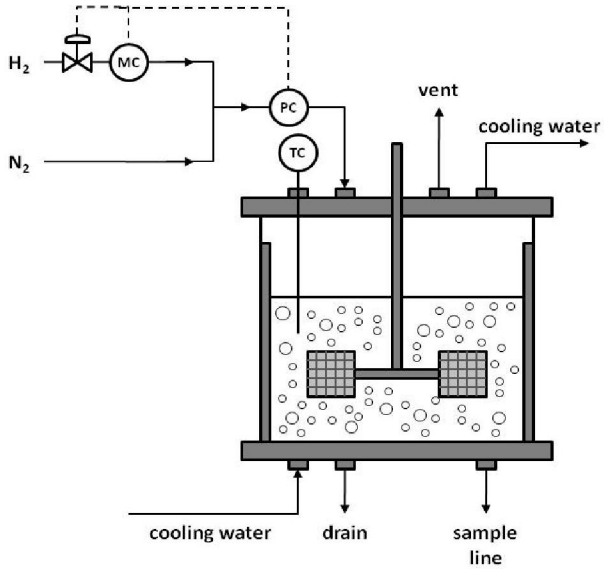

Figure 20: Schema of the autoclave reactor

Therefore, the balance in the bulk liquid phase for the hydrogen is not needed, since the hydrogen pressure is kept constant. The saturation concentration for the hydrogen assumed was calculated by Henry' law.

$$p_H = H.C_H^{sat} \qquad (3.9)$$

Where, p_H is the hydrogen pressure in the reactor, H represents the Henry's constant and C_H^{sat} the saturation concentration of hydrogen in the bulk liquid.

For the styrene in the bulk liquid, the mass balance takes the following expression:

$$\frac{dC_{Sty}^b}{dt} = -k_{ls}^{sty}.a_{ls}.\left(C_{Sty}^b - C_{Sty}^s\right); \frac{mol}{m_L^3 s} \quad (3.10)$$

Where k_{ls} ($m_{Liq\text{-}Sol}.s^{-1}$) correspond to the liquid – solid mass transfer coefficient, a_{ls} ($m_{Liq-Sol.}^2.m_{Liquid}^{-3}$) the liquid – solid mass transfer area per liquid volume, C_i^b and C_i^s ($mol.m^{-3}$) are the concentration of each component in the bulk liquid and at the liquid – solid interface, respectively.

Secondly, for the balance in the liquid-solid interface, it is considered the transport of styrene and hydrogen from the bulk liquid to the catalyst surface and the amount that reacts inside the catalyst. The diffusion resistance in the porous is expressed by the effectiveness factor.

The mass balance for the hydrogen and styrene is show respectively:

$$\varepsilon_S.\varepsilon_{Cat}.\frac{dC_H^s}{dt} = \varepsilon_L k_{ls}^{sty}.a_{ls}.(C_H^{sat} - C_H^s) - W_{cat}.(-r_H); \frac{mol}{m_R^3 s} \quad (3.11)$$

$$\varepsilon_S.\varepsilon_{Cat}.\frac{dC_{Sty}^s}{dt} = \varepsilon_L k_{ls}^{sty}.a_{ls}.\left(C_{Sty}^b - C_{Sty}^s\right) - W_{cat}.\left(-r_{Sty}\right); \frac{mol}{m_R^3 s} \quad (3.12)$$

Where $W_{cat}$is the mass of palladium in the reactor and ε_S ($m_{Solid}^3.m_{Reactor}^{-3}$), ε_{Cat} $\left(m_{Liquid.Cat}^3.m_{Solid}^{-3}\right)$, and ε_L($m_{Liquid}^3.m_{Reactor}^{-3}$) are the solid fraction, catalyst porosity and liquid fraction, respectively.

This model is fitted to experimental data, in order to estimate the liquid – solid mass transfer coefficient. The influence of stirring speed and foam ppi on this parameter is studied.

3.4. External mass transfer regime – parameter estimation

The model described previously allows estimate the mass transfer parameter and simulate the concentration of hydrogen and styrene at the catalyst surface. Figure 21 is an example of the model fitting to an experimental data and the simulation of the reactants concentration in bulk liquid and solid surface. The others results of model fitting are present in Annex B.

Firstly, the graph shows a good fitting, proving the accuracy of the model. Furthermore, it can be easily observed that, for the experimental conditions, the gradient of hydrogen concentration, between bulk liquid and the solid surface, is 5 times lower than for the styrene. However, at the end of the reaction, when the styrene concentration is too low, the situation changes, but is not easily to measure in the overall reaction.

Therefore, at this high initial concentration of styrene used, the liquid – solid mass transfer resistance is caused mainly by the hydrogen.

This means that the liquid – solid mass transfer coefficient for the hydrogen can be estimated precisely.

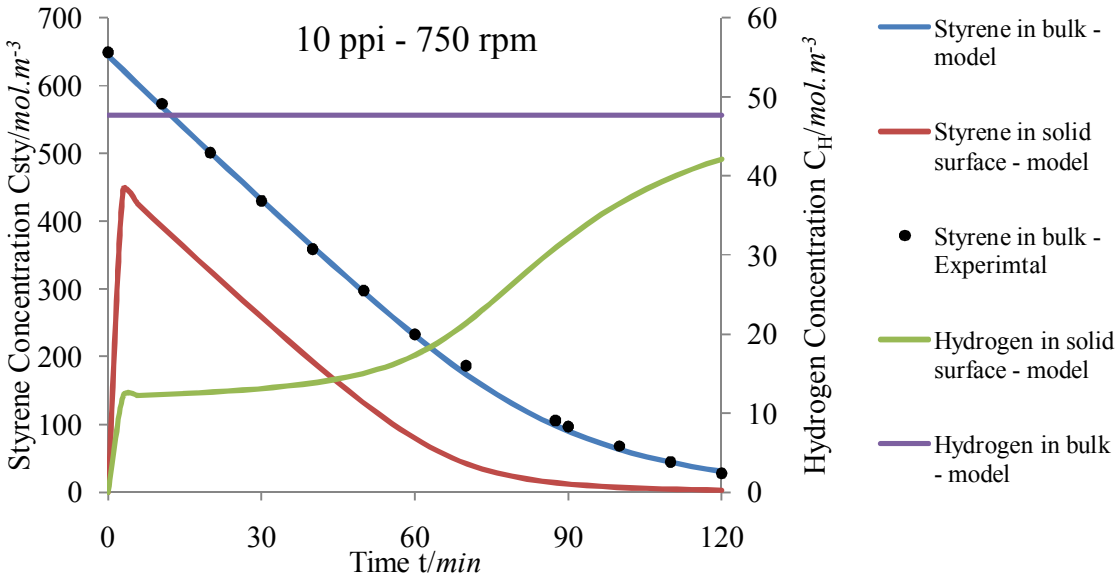

Figure 21: Concentration of reactants, experimental an predicted by the model, along the time, at 333K, Hydrogen pressure of 15 bars, with a palladium concentration of 12 $g.m_L^{-3}$, area per liquid volume equal to 2.8 $mg_{Pd}.g_{foam}^{-1}$ and a volume of liquid with $1.5x10^{-3}$ m_L^3- 10 ppi at 750 *rpm*.

In order to study the liquid – solid mass transfer, the volumetric and the intrinsic liquid – solid mass transfer were estimated for different stirring speeds and different foam ppi.

The reactions were carry out at 333 *K*, at a pressure of hydrogen 15 *bar*, 2 foam blades and with an initial concentration of styrene equal to 650 $mol.m_L^{-3}$. Furthermore, the palladium concentrations used for the 10, 20 and 40 ppi foam were 12, 21 and 16 $g.m_L^{-3}$, respectively.

Figure 22 presents the volumetric mass transfer coefficient estimated for hydrogen, $a_{LS}.k_{LS}$. It can be seen that there is a linear tendency in the increase of the $a_{LS}.k_{LS}$ with the stirring speed, which is directly related to the intrinsic velocity through the foams.

However, comparing the results for the different ppi foams, the $a_{LS}.k_{LS}$ for 40 ppi is almost 3 times higher than that for 10 and 20 ppi. Moreover, these two last have similar $a_{LS}.k_{LS}$ values at the same stirring speed.

This trend is not in agreement with previous studies carried out by Wenmakers [27]. Although he reported similar values of $a_{LS}.k_{LS}$ for 10 and 20 ppi foams as those shown in Figure 22, for the 40 ppi foam, a decrease of $a_{LS}.k_{LS}$ was found by Wenmakers.

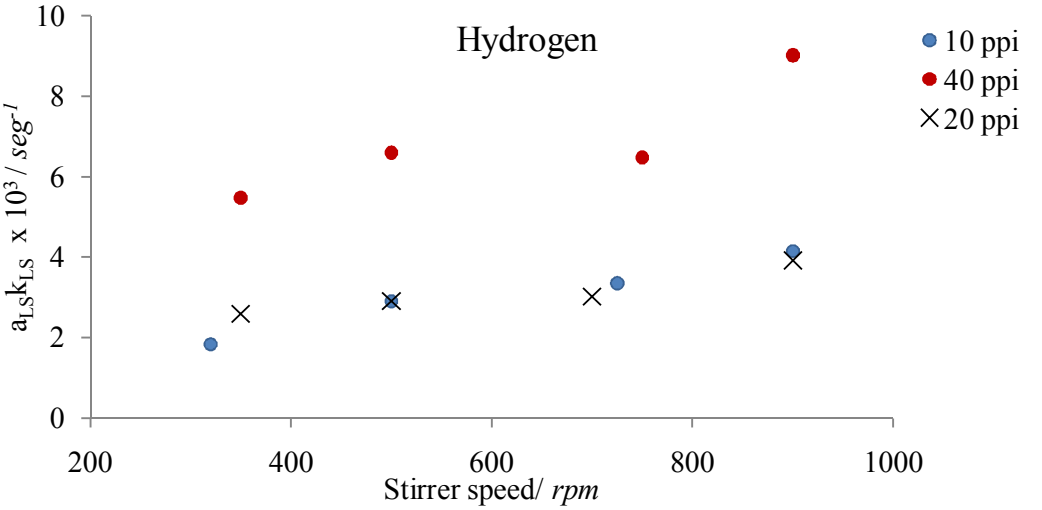

Figure 22: Volumetric liquid – solid mass transfer coefficient for different stirrer speed and for 2 active foams with different ppi number.

In order to support and complete the discussion, Figure 23 contains the intrinsic liquid – solid mass coefficient, k_{LS}, for hydrogen at different stirrer speed. Figure 23 shows the linear tendency between k_{LS} and the stirring speed. The increase of stirring

speed is proportional to the intrinsic velocity in the foam, which is, at same time, proportional to the intrinsic liquid – solid mass transfer as well.

When comparing the results obtained with 10 and 20 ppi foam, it can be observed a decrease of k_{LS} with 20 ppi. This decrease of k_{LS} value was expected due to the decrease of foam pore diameter, which increases the pressure drop and thus decrease the flow thought the foam. This leads to a decrease of intrinsic velocity on the foam surface and therefore to a lower value of k_{LS}.

However, since the 20 ppi foam has a higher area per foam volume, this explains the same value for the volumetric liquid – solid mass transfer coefficient as those obtained with 10 ppi foam.

On the other hand, the values of k_{LS} for foam with 40 ppi are between those obtained for 10 and 20 ppi foams. A lower value than the 20 ppi foam was expected due to the decreasing of intrinsic velocity on the foam surface by the higher pressure drop created by the smaller pores.

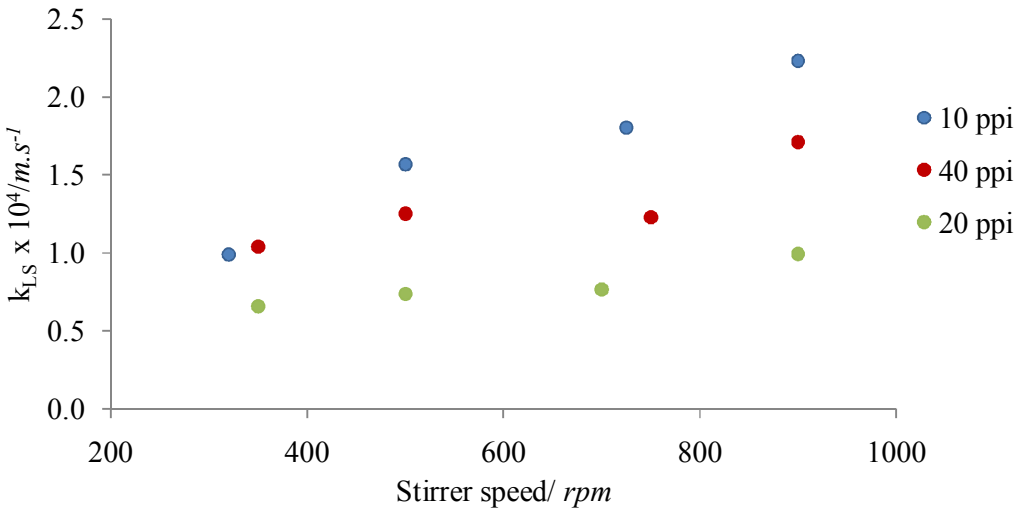

Figure 23: Liquid – solid mass transfer coefficient for different stirrer speed and for foams with different ppi's number.

The intrinsic liquid – solid mass transfer coefficients estimated in this project was between 0.5 x 10^{-4} and 2.5 x 10^{-4} $m.s^{-1}$.

Tschentscher et al. [9] studied the liquid – solid mass transfer for different reactor designs, slurry reactor and rotating block foam reactor. They reported, however, values, of k_{LS}, around 3 x 10^{-3} $m.s^{-1}$ for slurry reactor and 2.5 x 10^{-3} $m.s^{-1}$ for the rotating block foam reactor for lower stirring speed, between 100 and 400 *rpm*. They also mentioned

that the common values for industrial supported powders are 10 times lower. Actually the hydrodynamic of the reactor design present in this project is completely different from the rotating block foam reactor. Higher turbulence and area per volume of liquid are expected for rotating block foam reactor.

According with this paper, the reactor design used in this work shows mass transfer rate 10 times lower than the foam block used by Tschentscher. This suggests that the foam blade stirrer used does not promote the hydrodynamic necessary to compete with the slurry reactor.

In order to improve the hydrodynamic of rotating foam reactors, different stirrer designs could be considered like changing the number of blades, e.g. four foam blades placed in one plane or create a catalytic stirrer reactor with the foam structures in a vertical mode with the reactor vessel in a horizontal manner, in this way, the foams alternatively enter the liquid and the gas phase.

4. Conclusions

The first part of the project focused on the catalyst preparation using aluminium foams. This preparation involved three steps: anodization, washcoating and palladium impregnation.

In order to characterise the foam after those steps, two different techniques were used: SEM and TEM. The images captured by SEM showed a homogeneous alumina coating with thickness a little bit lower than the thickness estimated by gravimetric methods, considering an ideal distribution. This difference is caused by the accumulation of coating on the strut corners. This issue was more significant for foams with higher ppi number because the number of struts is higher. For 10, 20 and 40 ppi foams the average thickness reached was around 17, 24 and 35 μm, respectively. Also, when applied 2 and 3 washcoating to 10 ppi foams the thickness average increase to 43 and 94 μm, respectively.

Secondly, the TEM images showed a homogeneous distribution of palladium in the foam. All the catalyst prepared exhibited a narrow particle size distribution with an average diameter equal to 2.2 nm.

The second part of the project dealt with studying the performance of the foam catalyst in a multiphase reaction and the influence of liquid – solid mass transfer.

Firstly, the reaction was carried out with the inhibitor, tert-butlycatechol, in order to avoid some polymerization of styrene. However, the catalyst activity observed was 7 times lower than without inhibitor.

Secondly, in order to study the deactivation of the catalyst, the reaction was repeated with the same foam at same conditions but regenerating the catalyst at 120$^{\circ}C$ for 2 hours. Lower deactivation was observed after have used the catalyst two times. However, the following reactions showed the same activity. The decrease of activity in the second reaction is caused by the removal of some catalyst layer due to high stirring speed that was not well adherent to the support.

Afterwards, the kinetic of the reaction was studied. Activation energy of 54 kJ was found which is in the same range as reported by other authors.

Then, the reaction was carried out with liquid – solid mass transfer resistance for hydrogen. The range of values for intrinsic and volumetric liquid – solid mass transfer coefficient found was between $0.5x10^{-4}$ and $2.5x10^{-4}$ $m.s^{-1}$, and 2×10^{-3} and 1×10^{-2} $m_{LS}^{3}.m_{L}^{-3}.seg^{-1}$, respectively.

Those values are similar to those found in literature for common industrials slurry particles but they are 10 times lower than the ones reported for the rotating block foam reactor. This could be explained by the difference in hydrodynamics when changing the foam stirrer configuration.

When comparing the intrinsic liquid solid mass transfer for 10, 20 and 40 ppi foams, an unexpected trend was found. The intrinsic liquid – solid mass transfer coefficients for 40 ppi foams were lower than 10 ppi but higher than 20 ppi. It was expected that 40 ppi exhibits the lowest coefficient due to the lower intrinsic velocity caused by higher pressure drops on the small pores.

5. Suggestions for future works

In order to complete the liquid – solid mass transfer study, the reaction could be carried out at lower styrene concentration, like 10 times less. In this way, the limiting component in the liquid – solid mass transfer will be the styrene. Hence, intrinsic liquid-solid mass transfer coefficient for styrene can be estimated.

Moreover, internal mass transfer studies could be performed in order to optimize the alumina coating thickness to be deposited on the foam. For that the reaction should be carry out with different coating thickness. This can be done by increasing the washcoat layers.

Finally, the reaction could be performed at lower hydrogen pressure to measure the gas – liquid mass transfer resistance.

Since the intrinsic liquid – solid mass transfer obtained for this reactor configuration was lower than the one reported for the foam block, a study with a different foam blade configuration could be done, e.g. a stirrer having foam blades placed in a vertical mode while the reactor vessel is in an horizontal position.

In order to understand better how the hydrodynamics affects the k_{LS} value, the reaction could be done with different reactor design. For that some parameters should be tested as diameter of reactor, distance between the foam and the reactor wall.

Annex A: Proprieties of used foams

Table a: Principal characteristics of the catalysts used for different experiments.

Foam	Foam mass m_{Foam}/g	Foam ppi	Layers	Average Thickness average $L/\mu m$	Palladium mass m_{Pd}/mg
$F_{10} - X_1 - a$	1.8822	10	1	19	6.1
$F_{10} - X_1 - b$	1.9337	10	1	18	5.9
$F_{10} - X_2$	3.2692	10	1	12	6.9
$F_{10} - X_3$	4.0744	10	2	44	26.3
$F_{10} - X_4$	4.3199	10	2	41	26.9
$F_{10} - X_6$	5.2044	10	3	85	54.2
$F_{10} - X_7$	5.4587	10	3	102	63.9
$F_{10} - X_8$	3.6725	10	1	12	7.5
$F_{10} - X_9$	3.6146	10	1	18	11.2
$F_{10} - X_{10}$	4.1047	10	1	26	17.1
$F_{10} - X_{11}$	3.6523	10	1	14	8.8
$F_{20} - X_1$	3.7261	20	1	21	13.0
$F_{20} - X_2$	3.7575	20	1	29	17.4
$F_{20} - X_3$	3.9503	20	1	21	14.0
$F_{40} - X_2$	3.7095	40	1	44	24.2
$F_{40} - X_3$	3.7423	40	1	39	26.3
$F_{40} - X_4$	3.5703	40	1	23	28.1

Table b: Characteristics of the different ppi's foams

Ppi number	10 ppi	20 ppi	40 ppi
Surface area $m_{surface}^2/m_{foam}^{-3}$	800	1700	2600
Aluminium Density kg/m_{solid}^{-3}	2700	2700	2700
Porosity	0.93	0.93	0.93
Density apparent kg/m_{foam}^3	189	189	189
Dimensions xyz / *cm.cm.cm*	3.5 x 4.0 x 1.0		

Annex B: Experimental data and correspondent model fitting

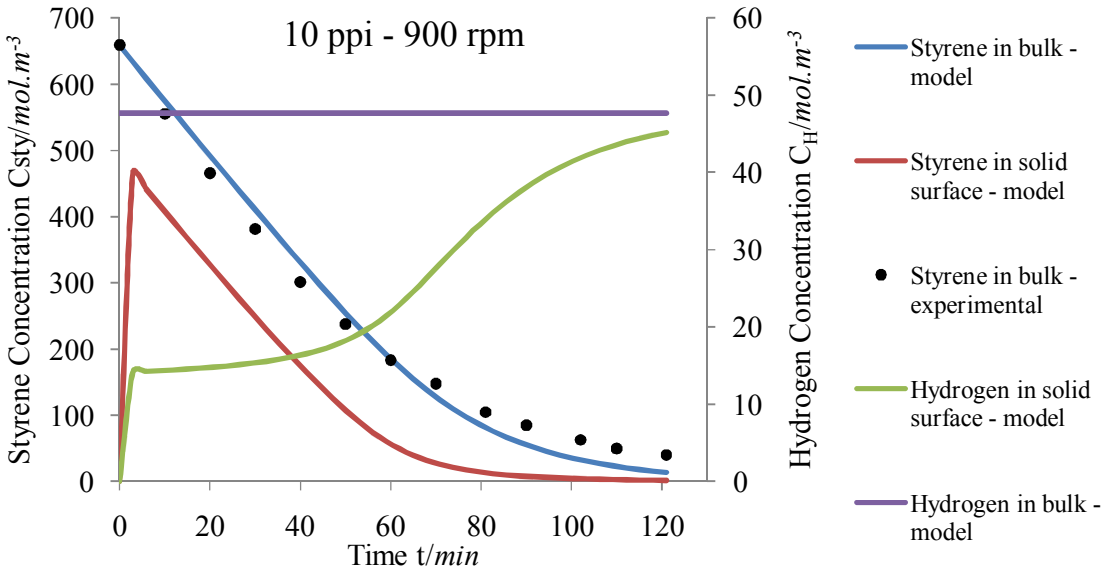

Figure a: Concentration of reactants, experimental an predicted by the model, along the time, at 333K, Hydrogen pressure of 15 bars, with a palladium concentration of 12 $g.m_L^{-3}$, area per liquid volume equal to 18.6 $m_{LS}^2.m_{Liq}^{-3}$ and a volume of liquid with 1.5x10^{-3} m_L^3 - 10 ppi foam at 900 rpm.

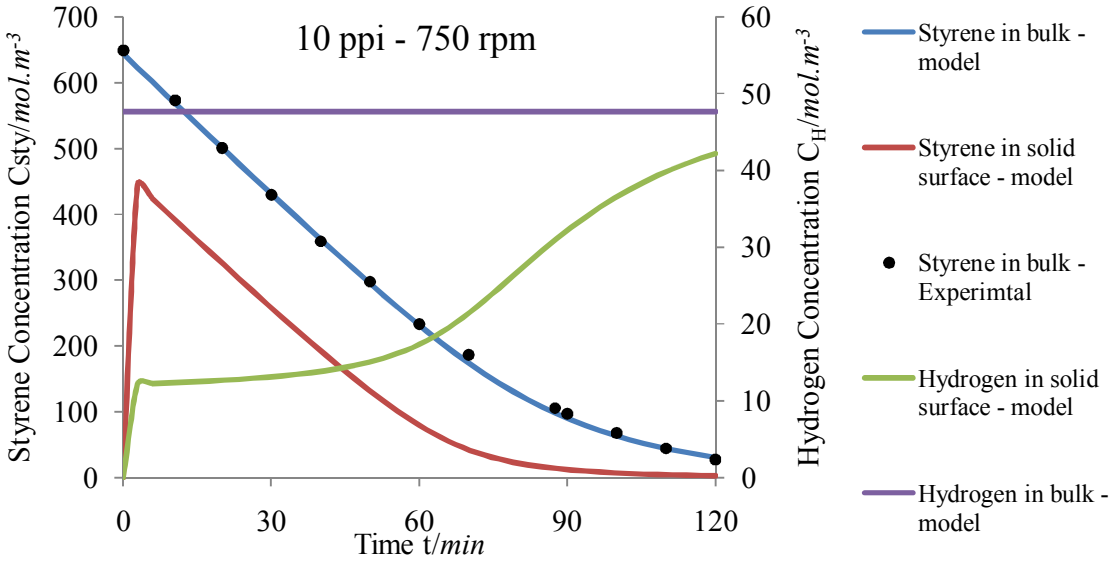

Figure b: Concentration of reactants, experimental an predicted by the model, along the time, at 333K, Hydrogen pressure of 15 bars, with a palladium concentration of 12 $g.m_L^{-3}$, area per liquid volume equal to 18.6 $m_{LS}^2.m_{Liq}^{-3}$ and a volume of liquid with 1.5x10^{-3} m_L^3 - 10 ppi foam at 750 rpm.

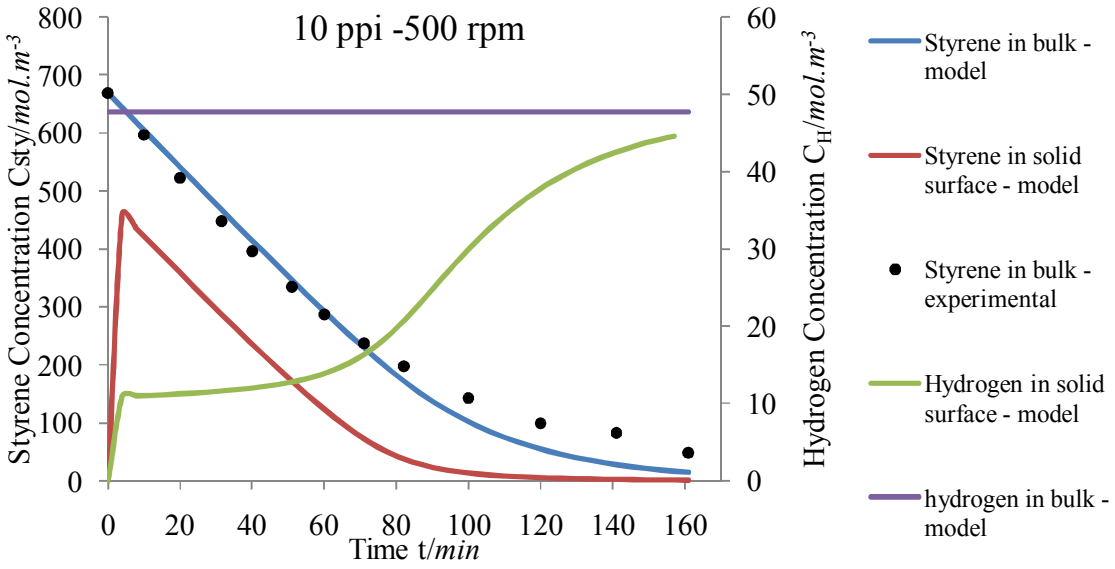

Figure c: Concentration of reactants, experimental an predicted by the model, along the time, at 333K, Hydrogen pressure of 15 bars, with a palladium concentration of 12 $g.m_L^{-3}$, area per liquid volume equal 18.6 $m_{LS}^2.m_{Liq}^{-3}$ and a volume of liquid with $1.5x10^{-3}$ m_L^3 - 10 ppi foam at 500 rpm.

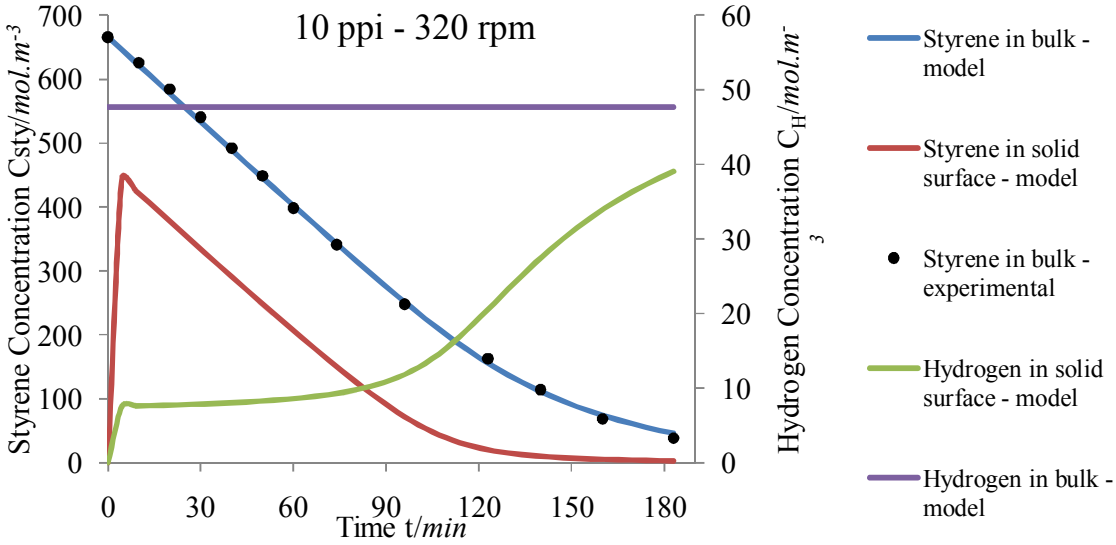

Figure d: Concentration of reactants, experimental an predicted by the model, along the time, at 333K, Hydrogen pressure of 15 bars, with a palladium concentration of 12 $g.m_L^{-3}$, area per liquid volume equal to 18.6 $m_{LS}^2.m_{Liq}^{-3}$ and a volume of liquid with $1.5x10^{-3}$ m_L^3 - 10 ppi foam at 320 rpm.

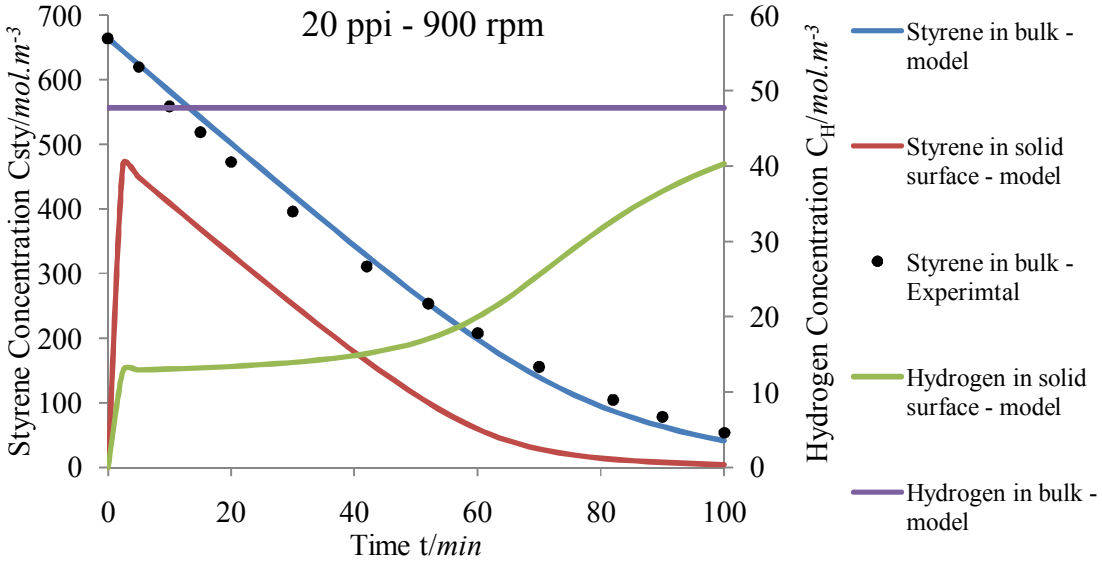

Figure e: Concentration of reactants, experimental an predicted by the model, along the time, at 333K, Hydrogen pressure of 15 bars, with a palladium concentration of 21 $g.m_L^{-3}$, area per liquid volume equal to 39.5 $m_{LS}^2.m_{Liq}^{-3}$ and a volume of liquid with $1.5x10^{-3}$ m_L^3 - 20 ppi foam at 900 rpm.

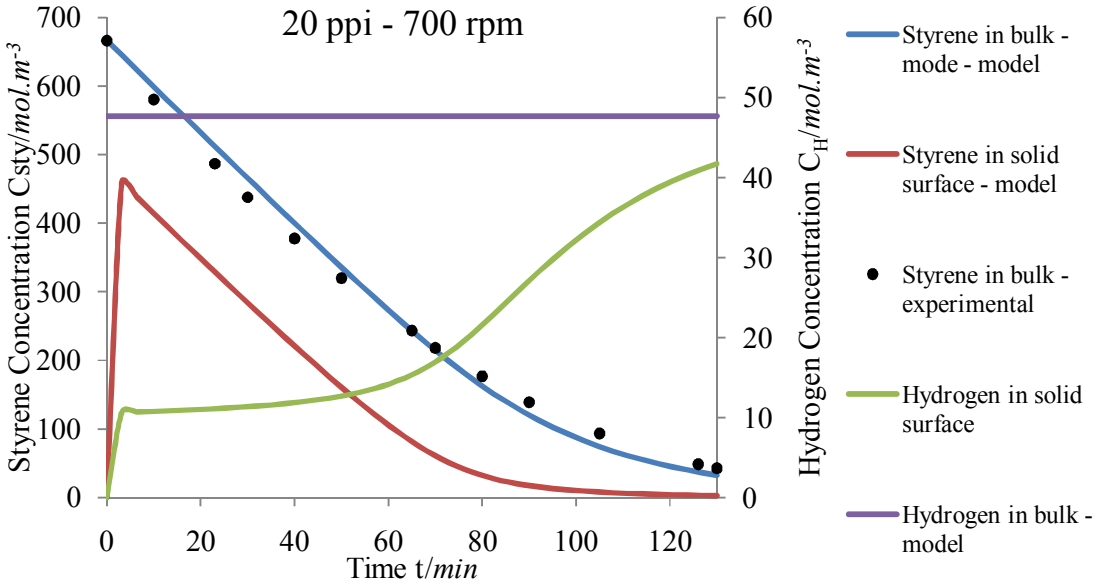

Figure f: Concentration of reactants, experimental an predicted by the model, along the time, at 333K, Hydrogen pressure of 15 bars, with a palladium concentration of 21 $g.m_L^{-3}$, area per liquid volume equal to 39.5 $m_{LS}^2.m_{Liq}^{-3}$ and a volume of liquid with $1.5x10^{-3}$ m_L^3 - 20 ppi foam at 700 rpm.

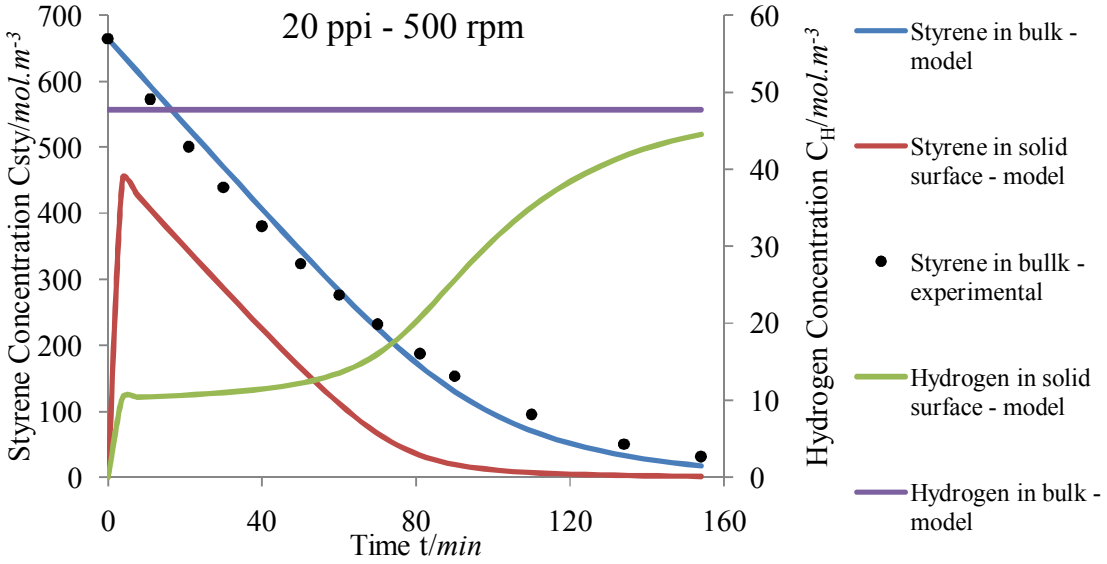

Figure g: Concentration of reactants, experimental an predicted by the model, along the time, at 333K, Hydrogen pressure of 15 bars, with a palladium concentration of 21 $g.m_L^{-3}$, area per liquid volume equal to 39.5 $m_{LS}^2.m_{Liq}^{-3}$ and a volume of liquid with $1.5x10^{-3}$ m_L^3.

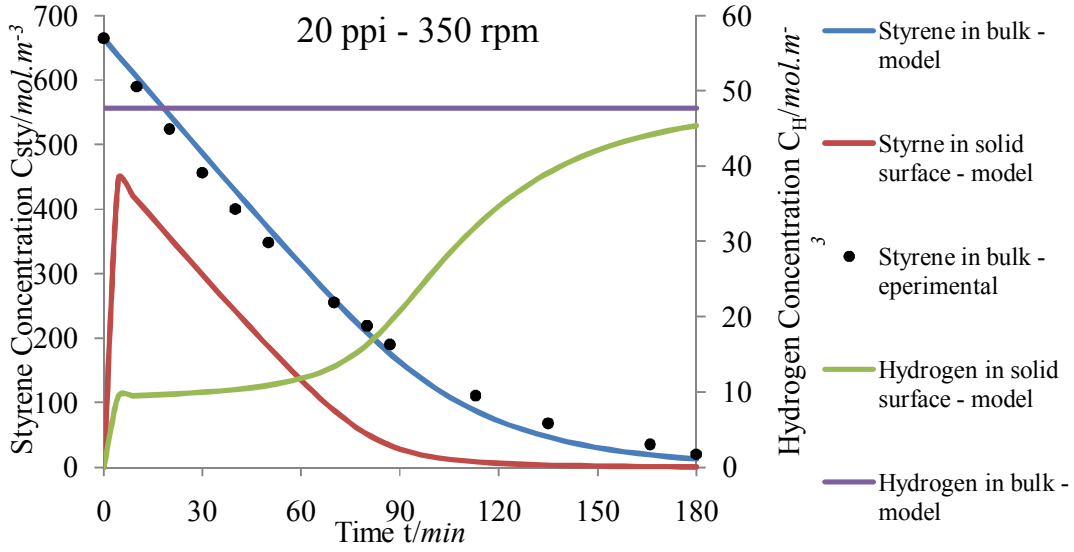

Figure h: Concentration of reactants, experimental an predicted by the model, along the time, at 333K, Hydrogen pressure of 15 bars, with a palladium concentration of 21 $g.m_L^{-3}$, area per liquid volume equal to 39.5 $m_{LS}^2.m_{Liq}^{-3}$ and a volume of liquid with $1.5x10^{-3}$ m_L^3 - 20 ppi foam at 350 rpm.

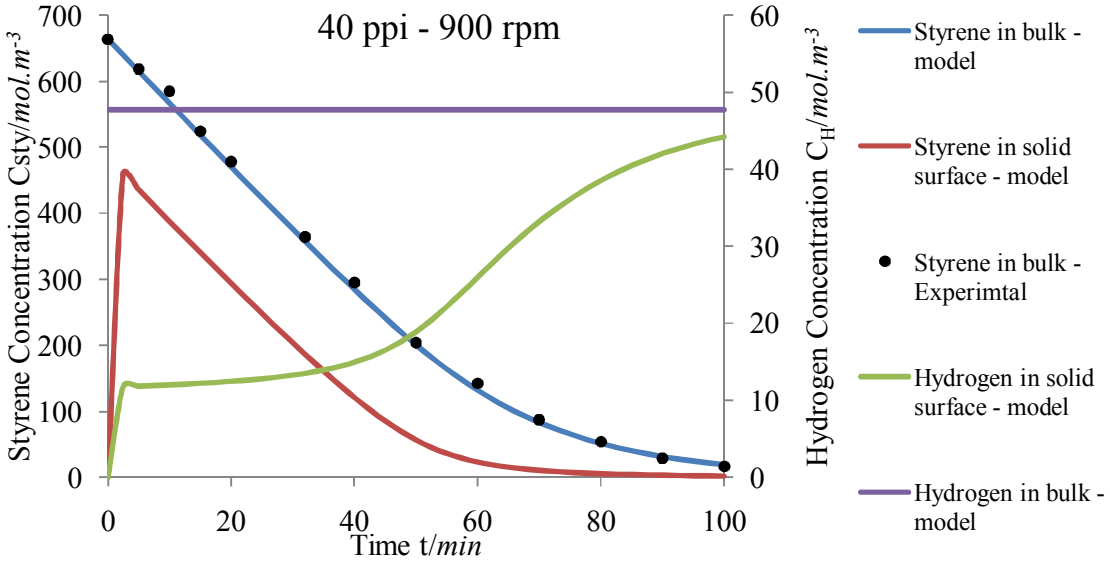

Figure i: Concentration of reactants, experimental an predicted by the model, along the time, at 333K, Hydrogen pressure of 15 bars, with a palladium concentration of 16 $g.m_L^{-3}$, area per liquid volume equal to 26.4 $m_{LS}^2.m_{Liq}^{-3}$ and a volume of liquid with $1.5x10^{-3}$ m_L^3 - 40 ppi foam at 900 rpm.

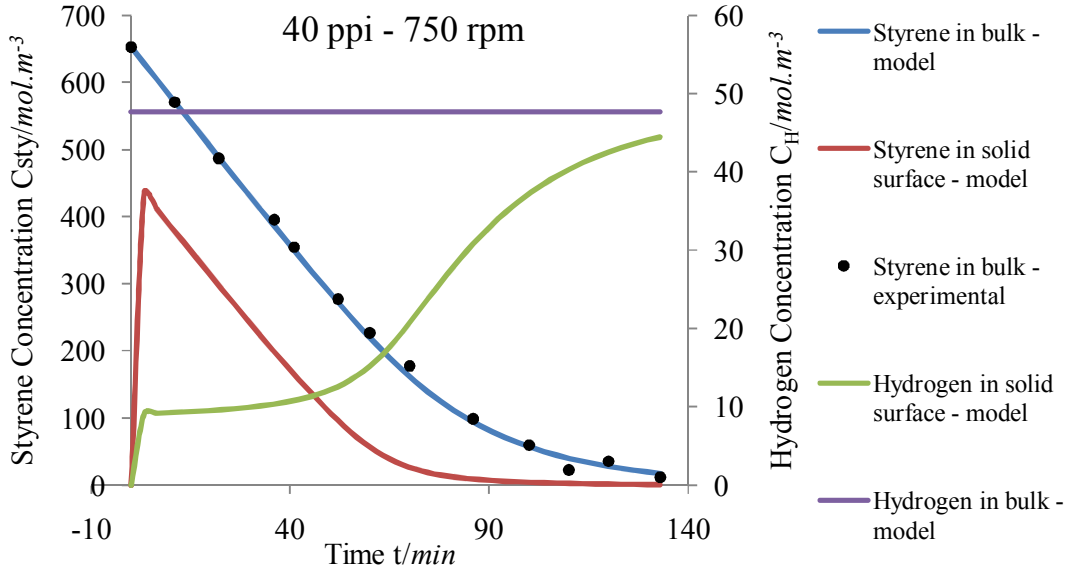

Figure j: Concentration of reactants, experimental an predicted by the model, along the time, at 333K, Hydrogen pressure of 15 bars, with a palladium concentration of 16 $g.m_L^{-3}$, area per liquid volume equal to 26.4 $m_{LS}^2.m_{Liq}^{-3}$ and a volume of liquid with $1.5x10^{-3}$ m_L^3 - 40 ppi foam at 750 rpm.

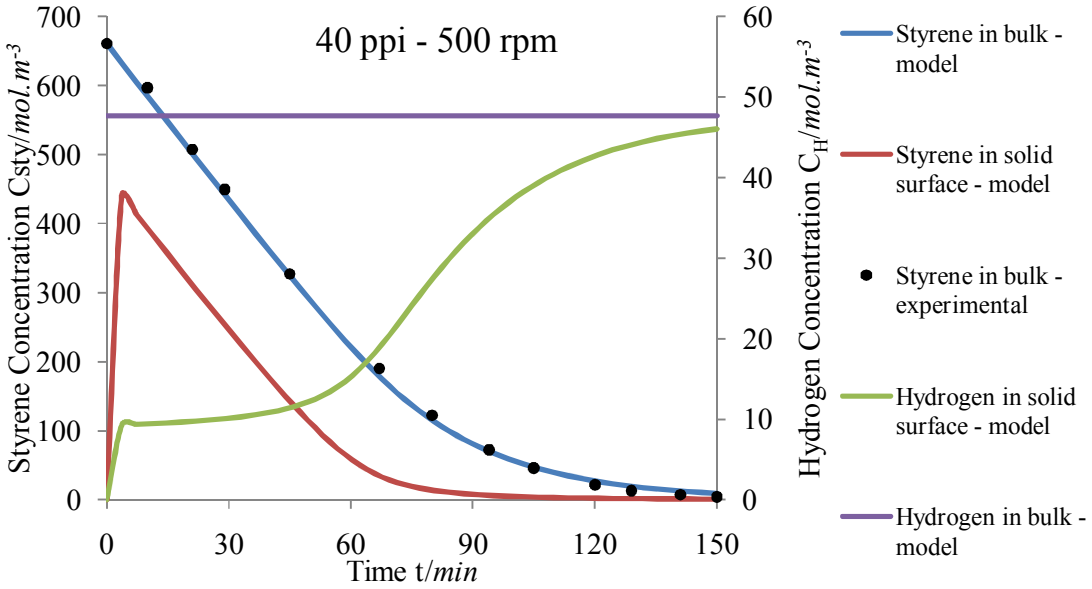

Figure k: Concentration of reactants, experimental an predicted by the model, along the time, at 333K, Hydrogen pressure of 15 bars, with a palladium concentration of 16 $g.m_L^{-3}$, area per liquid volume equal to 26.4 $m_{LS}^2.m_{Liq}^{-3}$ and a volume of liquid with $1.5x10^{-3}$ m_L^3 - 40 ppi foam at 500 rpm.

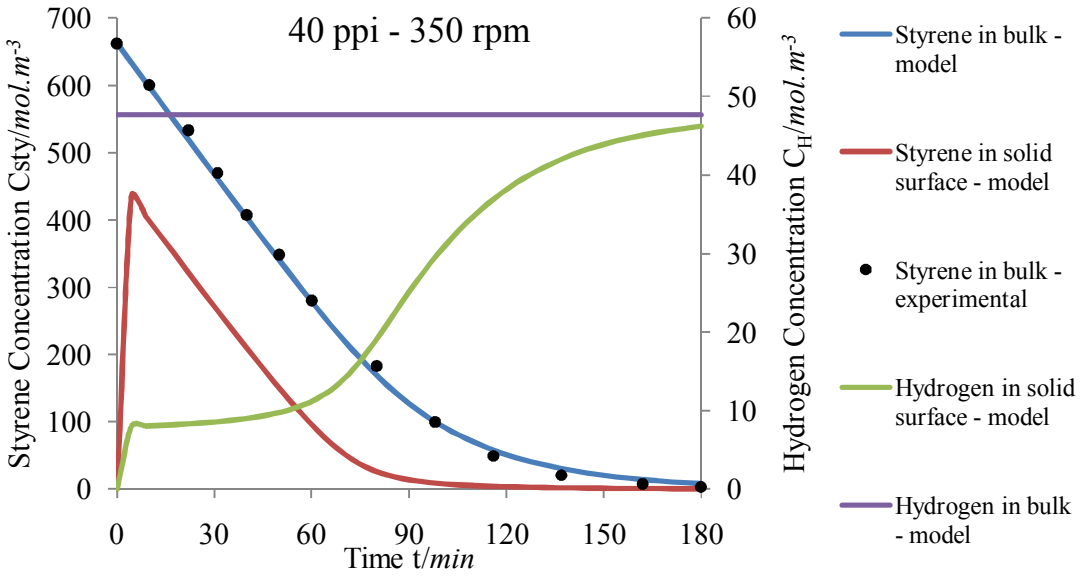

Figure l: Concentration of reactants, experimental an predicted by the model, along the time, at 333K, Hydrogen pressure of 15 bars, with a palladium concentration of 16 $g.m_L^{-3}$, area per liquid volume equal to 26.4 $m_{LS}^2.m_{Liq}^{-3}$ and a volume of liquid with $1.5x10^{-3}$ m_L^3 - 40 ppi foam at 350 rpm.

References

[1] R. Krishna, *Strategies for multiphase reactor selection*, Chemical Engineering Science, Vol. 49, pages 4029-4065, **1994**.

[2] I. Iliuta, F. Laracchi, B. Grandjean, G. Wild, *Gas – liquid mass transfer in trickle- bed reactors: state-of-the-art correlations*, Chemical Engineering Science, Vol. 54, pages 5633-5645, **1999**.

[3] F. Larachi, L. Belfares, I. Iluita, B. Grandjean, *Heat and mass transfer in Conurrent Gas – Liquid Packed beds, Analysis, Recommendations, and New Correlations*, Ind. Eng. Chem. Res., Vol. 42, pages 222-242, **2003**.

[4] T. Nijhuis, M. Kreutzer, A. Romijin, F. Kapteinjn, J. Moulijn, *Monolithic catalyst as efficient three-phase reactors*, Chemical Engineering Science, Vol. 56, pages 823-829, **2001**.

[5] I. Hoek, Towards the Catalytic Application of a Monolithic Stirrer Reactor, PhD thesis, Tu/delft, the Nedertlands, **2004**.

[6] T. Nijhuis, G. Koten, F. Kapteijn, J. Moulijn, *Separation of kinetics and mass-transport effects for a fast reaction: the selective hydrogenation of functionalized alkynes*, Catalysis Today, 79-80, pages 315-321, **2003**.

[7] T. Nijhuis, G. Koten, J. Moulijn, *Optimized palladium catalyst systems for the selective liquid-phase hydrogenation of functionalized alkynes*, Applied Catalysis A: General, Vol. 238, pages 259-271, **2003**.

[8] R. Tschentscher, T. Nijhuis, J. Schaaf, B. Kuster, J. Schouten, *Gas – liquid mass transfer in rotating solid foam reactors*, Chemical Engineering Science, Vol. 65, pages 472-479, **2010**.

[9] R. Tschentscher, R. Spijkers, T. Nijhuis, J. Schaaf, J. Schouten, Liquid – Solid Mass Transfer in Agitated Slurry Reactors and Rotating Solid Foam Reactors, **2009**.

[10] Y. Cheng, J. Chang, J. Wu, *Kinetic study of pyrolysis gasoline hydrogenation over supported palladium catalyst*, Applied Catalysis, Vol. 24, pages 273-285, **1986**.

[11] T. Nijhuis, F. Dautzenberg, J. Moulinjn, *Modeling of monolithic and trickle-bed reactors for the hydrogenation of styrene*, Chemical Engineering Science, Vol. 58, pages 1113-1124, **2003**.

[12] Z. Zhou, Z. Cheng, Y. Cao, J. Zhang, D. Yang, W. Yuan, *Kinetics of the selective Hydrogenation of Pyrolysis Gasoline*, Chem. Eng. Technol., Vol. 30, pages 105-111, **2007**.

[13] Z. Zhou, Z. Cheng, D. Yang, X. Zhou, W. Yuan, *Solubility of Hydrogen in Pyrolyses Gasoline*, J. Chem. Eng. Data, Vol. 51, pages 972-976, **2006**.

[14] R. Tschentscher, T. Nijhuis, J. Schaaf, B. Kuster, J. Schouten, *Preparation of Porous Alumina Coating on Aluminum Foams*, Applied Catalysis A: General, **2008**.

[15] L. Giani, C. Cristina, G. Groppi, E. Tronconi, *Washcoating method for Pd/γ-Al_2O_3 deposition on metallic foams*, Applied Catalysis B: Environmental, Vol. 62, pages 121-131, 2006.

[16] O. Sanz, L. Martínez, F. Echave, M. Domínguez, M. Centeno, J. Odriozola, M. Montes, *Aluminium anodization for Au-CeO2/Al2O3-Al monoliths preparation*, Chemical Engineering Journal, Vol. 151, pages 324-332, **2009**.

[17] O. Sanz, L. Almeida, J. Zamaro, M. Ulla, E. Míro, M. Montes, *Washcoating of Pt-ZSM5 onto aluminium foams*, Applied Catalysis B: Environmental, Vol. 78, pages 166-175, **2008**.

[18] N. Fígoli, P. L'Argentiere, *Deactivation of sulfur-poisoned supported palladium complexes*, Journal of Molecular Catalysis A: Chemical, Vol. 122, pages 141-146, **1997**.

[19] P. L'Argentiere, N. Fígoli, Regeneration of a Sulfur Poisoned Pd/AL_2O_3 Catalyst during the selective Hydogenation of Styrene, Applied Catalyst, Vol. 61, pages 275-282, **1990**.

[20] M. Semsarzadeh, M. Abdollahi, *Atom Transfer Radical Homo- and Copolymerization of Styrene and Methyl Acrylate Initiated with Trichloromethyl- Terminated Poly(vinyl acetate) Macroinitiator: A Kinetic Study*, Journal of Applied Polymer Science, Vol. 114, pages 2509 – 2521, **2009**.

[21] G. Ertl, H. Kenözinger, F. Schüth, J. Weitkamp, *Handbook of Heterogeneous Catalysis*, Vol. 3, 2th edition, Wiley-VCH, **2008**.

[22] S. Jackoson, L Shaw, *The liquid-phase hydrogenation of phenyl acetylene and styrene on a palladium/carbon catalyst*, Applied Catalysis A: General, Vol. 134, pages 91-99, **1996.**

[23] R. Chaudhari, R. Jaganathan, S. Kolhe, G. Emig, F. Hofmann, *Kinetic modelling of a complex consecutive reaction in a slurry reactor: hydrogenation of phenyl acetylene*., Chemical Engineering Science, Vol. 41, pages 3073-3081, **1986**.

[24] *Perry's chemical engineer's handbook,* 7th edition, McGraw-Hill, international edition, **1997**.

[25] F. Santos, C. Castro, *Standard reference data for the viscosity of Toluene.,* J. Phys. Chem. Ref. Data, Vol. 35, No. 1, **2006**.

[26] Octave Levenspiel, *Chemical Reactor Engineering*, 3th edition, John Wiley & Sons, Inc., **1999**.

[27] Patrick Wenmakers, *Hairy Foam: Carbon nanofibers on solid as catalyst support – Synthesis, mass transfer and reactor modeling.,* 1th Edition, Technische Universiteit Eindhoven, **2009**.